Sheet thickness dependence of magnetization properties based on domains and walls within the non-linear diffusion-like equation for Grain-Oriented Electrical Steels

Olivier Maloberti, Elias Salloum, M L Ababsa, Manar Nesser, Stéphane Panier, Pascal Dassonvalle, Jérôme Fortin, C Pineau, J-P Birat

Graphical Abstract

To create your abstract, type over the instructions in the template box below.
Fonts or abstract dimensions should not be changed or altered.

Sheet thickness dependence of magnetization properties based on domains and walls within the non-linear diffusion-like equation for Grain-Oriented Electrical Steels

O. Maloberti[1,2], E. Salloum[2], M.L. Ababsa[1,4], M. Nesser[2], S. Panier[2], P. Dassonvalle[1,3], J. Fortin[2], C. Pineau[5], J-P. Birat[6]

[1]*ESIEE-UNILASALLE Amiens, 14 quai de la Somme, 80080 Amiens, France*
[2]*LTI Laboratory, Avenue des Facultés - Le Bailly 80025 Amiens, France*
[3]*MIS laboratory, UPJV, 14 Quai de la Somme, 80080 Amiens, France*
[4]*LSEE Lab., Faculté des Sciences Appliquées, Technoparc Futura, 62400 Béthune, France*
[5]*IRT-M2P, 4 rue Augustin Fresnel, 57070 Metz, France*
[6]*IF Steelman, 5 rue du Gate Chaux, 57280 Semecourt, France*

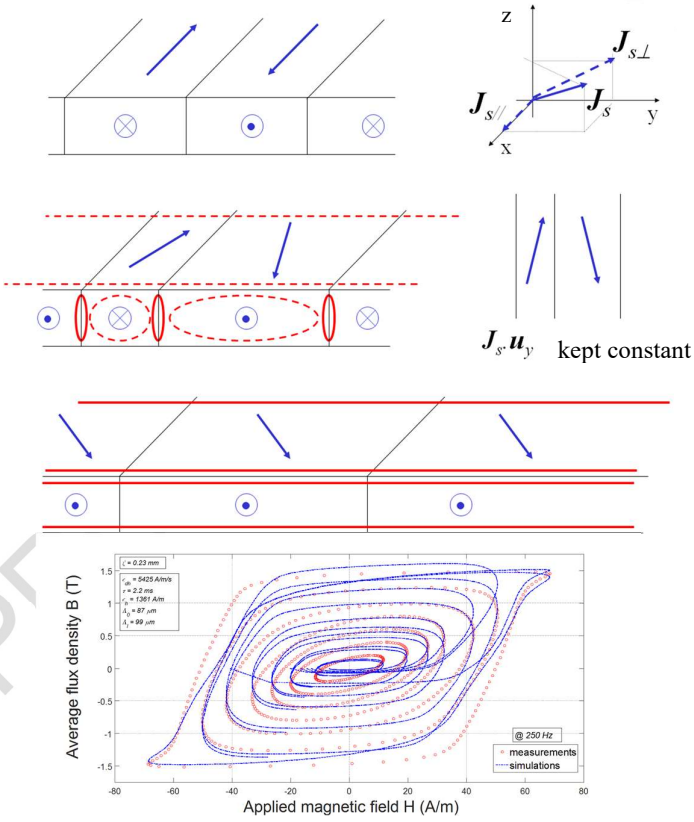

Journal of Magnetism and Magnetic Materials
journal homepage: www.elsevier.com

Sheet thickness dependence of magnetization properties based on domains and walls within the non-linear diffusion-like equation for Grain-Oriented Electrical Steels.

O. Maloberti[1,2], E. Salloum[2], M L Ababsa[1,4], M. Nesser[2], S. Panier[2], P. Dassonvalle[1,3], J. Fortin[2], C. Pineau[5], J-P. Birat[6].

[1]*ESIEE-UNILASALLE Amiens, 14 quai de la Somme, 80080 Amiens, France*
[2]*LTI Laboratory, Avenue des Facultés - Le Bailly 80025 Amiens, France*
[3]*MIS laboratory, UPJV, 14 Quai de la Somme, 80080 Amiens, France*
[4]*LSEE Lab., Faculté des Sciences Appliquées, Technoparc Futura, 62400 Béthune, France*
[5]*IRT-M2P, 4 rue Augustin Fresnel, 57070 Metz, France*
[6]*IF Steelman, 5 rue du Gate Chaux, 57280 Semecourt, France*

ARTICLE INFO

Article history:
Submitted

Keywords:
Electrical steels
Iron Losses
Apparent permeability
Dynamic hysteresis
Magnetic domains and walls
Domain Walls Displacement
Domains Magnetization Rotation
Magnetization curves
Magnetic field damping
Eddy currents
Field diffusion equation
Domains refinement
Walls' mobility
Surface magnetic poles
Surface closure domains

ABSTRACT

The definition and development of a dynamic or transient magnetic formulation compatible with the Finite Element Method, able to take the dynamic hysteresis and classical and extra losses into account (not *a posteriori* but *a priori*), and using the most adapted state variable that makes the problem well defined and easily convergent requires the knowledge of dynamic behavioral properties of soft magnetic materials whatever the thickness and the working conditions. The dynamic hysteresis of soft magnetic materials corresponds to excess iron losses, due to dynamic magnetization reversal processes within magnetic domains and especially to microscopic eddy currents around the magnetic walls in motion and inside rotating domains. The model properties used are the internal quasi-static permeability μ and the dynamic magnetization property Λ that lumps the magnetization mechanisms (domain walls displacement, bowing, fusion, nucleation and multiplication). The latter are involved in the magnetic field damping due to microscopic eddy currents within the field diffusion that renders the magnetic behavior geometry dependent. This model does not separate the field diffusion process from the magnetization reversal mechanisms. In this paper, the sheet thickness ζ dependence of the dynamic magnetization property $\Lambda(\zeta)$ for a Grain Oriented Electrical Steel (GOES: steel made of 3% Silicon and Iron: SiFe) is analyzed in the Rolling Direction (RD). To this extend, it is proposed to carry out and interpret magnetic measurements on GOES samples with the Epstein frame for four different thicknesses ($\zeta = 0.23, 0.27, 0.30$ and 0.35 *mm*), but with similar metallurgical and crystallographic properties for the whole specimens. Magnetic properties are first identified at low induction with linear assumptions and at higher induction with non-linearities. It makes it possible to re-compute the dynamic hysteresis loops of the material and to predict the losses whatever the working conditions with frequencies from 50 to 800 Hz. It is found that μ does not depend significantly on the sheet thickness whereas Λ depends on it significantly. Microscopic observation of the magnetic domains width are then performed thanks to the MOIF (Magneto-Optical Indicator Film) technique. It helps us discriminate between three simultaneous origins for the dependence of iron losses to the sheet thickness: a skin-like effect, a domains' refinement and changes on the walls' mobility. Results are discussed taking the dipolar magnetic effects, closure domains, the grains and texture and the manufacturing and coating residual stress on the metal surface into account.

1. Introduction, State of The Art and Generalities

Iron losses and magnetic hysteresis of soft magnetic materials are mainly due to its microscopic magnetic structures with domains, walls, vortices and other microscopic magnetic objects in motion. These two phenomena have been studied for decades with numerous models, able to reproduce with physical significance and accuracy the experimental data. The first experimental studies onto the magnetic domains and walls have been carried out by references F. Bitter [1] at the end of the 19th century. Then, P. Weiss proposed his first theoretical hypothesis that led to the idea of magnetic domains in ferromagnetic materials [2, 3] at the beginning of the 20th century. Next, Pry & Bean [4] published their theoretical explanation of the connection between the motion of walls between the domains and the magnetic losses in the middle of the 20th century. Then several important authors have proposed very useful and powerful models, both physical and mathematical models, that are able to either predict with accuracy the magnetic losses or reproduce the corresponding magnetic behavior and hysteresis. Ch.P. Steinmetz [5, 6] was one of the first author to propose an empirical loss power law as a function of the induction B and the frequency f during the second half of the 20th century. A more complete and accurate loss power law has been

physically and theoretically analyzed and proposed by G. Bertotti [7, 8] at the end of the 20th century. The most recent and significant achievement concerning the loss prediction comes from the Loss-Surface model, called L-S model developed by A. Kedous-Lebouc [9]. The latter can also predict the dynamic hysteresis whatever the waveshape of flux density B [14]. The most famous hysteresis models are static hysteresis models: the Preisach model [10] and the Jiles Atherton model [12] for examples. However, each of these models has got its dynamic extension mainly thanks to the work of I.D. Mayergoyz and G. Bertotti [11, 13]. Most of these models have been proposed independently from the field equations, leading to an artificial separation between the magnetization reversal mechanisms and the field diffusion inside the material. Moreover, model parameters are not so easy to identify and the hysteretic material behavior *a posteriori* added to the field equations render the computations time consuming and hardly convergent. M.A. Raulet [15] was the first author to propose a dynamic field diffusion equation, *i.e.* a formulation that does not separate the effects of the magnetic structure and the effects of the field diffusion. However, this proposal still involves a non-univocal and non-explicit dynamic law that is again hardly convergent. To improve the physical interpretation of identifications and try to ease and speed up the calculations, the present study is closely related to the proposal to use a new energy formulation involving only univocal behavioral laws [16], while focusing on the dynamic losses and hysteresis [17]. It has been shown in reference [17, 25, 26] that this dynamic modeling can represent well NO SiFe steels. One of the goals of this paper is to examine the adequation of the dynamic model to GO SiFe steels and for various thicknesses.

The whole models should probably depend on several materials parameters related to crystallographic (easy axis, grains orientation and texture), metallurgical (grains size, joints and defects) and magnetic (saturation polarization, domains and walls size and mobility) properties even if we cannot always clarify this relationship. These last parameters are assumed to be intrinsic to the material itself. The local behavioral law associated to the Maxwell equations are then supposed to describe the global behavior of any sample; whatever the shape, the geometry and the size are. Nevertheless, other research clearly show that the magnetic domains size strongly depends on the grain and sample shape and dimensions [18]. The surface quality and roughness have also got a significant impact. In fact, the surface magnetic structure is mainly driven by the crystallographic texture, closure domains and the demagnetizing energy due to surface magnetic poles. The bulk magnetic structure then will be at its turn driven by the limit conditions imposed by the surface magnetic structure and the bulk crystallographic state and phases. Meanwhile, the walls mobility, pinning effects and nucleation are greatly influenced by the joints and defects distribution and the magnetic walls area [19]. Therefore, it is hardly said that the materials properties linked to its magnetic structure are intrinsic only to the material and not to the geometry. In most of previous loss and hysteresis models, including the one at the basis of present work, it is not so easy to justify and physically describe the impact of grains and sample shape, geometry and size onto its parameters. It means that two identical bulk alloys with two different shapes or/and dimensions will require two different sets of parameters to make the models usable. The same difficulty occurs for two identical alloys with two different surface qualities. The role played by the sample shape, geometry and size has been investigated and perfectly modelled mainly for small particles, single domains samples, permanent magnets or single crystals [18]. Some research has however been carried out to study the impact of one sample dimension [20-24]: the thickness of an electrical sheet. These investigations have been done thanks only to global loss or hysteresis measurements, without trying to identify any variations of models' parameters. M.A. Raulet [23] is the first author to have initiated the research on that subject. In the following, we will focus on the geometry dependence of the dynamic field diffusion like model, that makes a connection between the dynamic parameter and the microscopic magnetization reversal mechanisms. It is proposed to analyze the impact of a magnetic sheet thickness on models' parameters and to interpret the results at the microscopic scale for further investigations.

2. The magnetic field diffusion with domains and walls – Field diffusion-like equation

In this section, we introduce the complete magnetic model from reference [17, 25, 26], including its scalar dynamic magnetization property Λ to be associated to the internal static magnetic permeability μ, but with maximum consideration of magnetization reversal mechanisms with static and dynamic non-linearities that may occur in a Grain Oriented Electrical Steel (GOES) at various dynamic working conditions.

2.1. Static and dynamic magnetization

2.1.1. Magnetization reversal mechanisms

Magnetic structures involve mainly the magnetic domains, the domains walls and microscopic objects such as the vortices. Magnetization reversal mechanisms depend on the working conditions. One first kind of mechanism, major at low induction levels, is the **D**omain **W**alls **D**isplacement (DWD) with possible parallel mechanisms such as the **D**omain **W**alls **B**owing (DWB) and the **D**omain **W**alls **M**ultiplication (DWM). Then, additional magnetization mechanisms become significant at higher induction levels such as the **D**omains' **M**agnetization **R**otation (DMR) accompanied by the **D**omain **W**alls **N**ucleation (DWN) and the **D**omain **W**alls **F**usion (DWF). The DMR Domains Magnetization Rotation is highly negligible in front of DWD Domains Walls Displacement at induction levels below saturation. However, it becomes significant when the magnetization approaches the knee and saturation level due to fusion of walls, which can occur even with a relatively low magnetic field above H~25 A.m^{-1} thanks to the very high permeability of such materials. There, the walls disappear progressively, it becomes necessary for the material to use the DMR process in order to increase again the magnetization, which involves higher applied magnetic fields (up to 100 A/m) to be added to the local and internal demagnetizing or grains shape anisotropy field. Moreover, at high enough induction level, the DMR process becomes significant. Comparisons of the DMR and the DWD processes and corresponding eddy currents as a function the induction level and frequency can be found in several references [25, 31], and they all lead to the same conclusion: the description of magnetization dynamics and losses at high induction levels must take the whole mechanisms including the DWD with bowing (DWB), multiplication (DWM), fusion (DWF), nucleations (DWN) and the DMR process.

The global mesoscopic magnetic polarization along the walls' direction $J_{//}$ can be expressed as a function of the active walls density n_{wa}, surface A_w and relative position x_w such that its velocity $v_w = \partial_t x_w$. Depending on the magnetic field direction and partly due to the combination of residual stress and shape anisotropies next to the field coupling, saturation polarization $\boldsymbol{J}_s$ of non perfectly orientated domains can make a small angle with the walls' direction, *i.e.* with $J_{s\perp}$ a component of $\boldsymbol{J}_s$ perpendicular to the walls' direction (Figure 1).

$$J_{//} \cdot \frac{1}{n_{wa} A_w} = 2\sqrt{J_s^2 - J_{s\perp}^2} \cdot \int v_w dt \qquad (1)$$

The change in magnetic polarization inside the material with various domains more or less well oriented due to the various mechanisms can then be deduced thanks to a time derivative of equation (1):

$$\partial_t J_{//} = 2\sqrt{J_s^2 - J_{s\perp}^2}.n_{wa}A_w v_w + \frac{J_{//}.\partial_t\left(\sqrt{J_s^2-J_{s\perp}^2}\right)}{\sqrt{J_s^2-J_{s\perp}^2}} \tag{2}$$

Microscopic eddy currents $j_{\mu w}$ and $j_{\mu d}$ are induced around moving domain walls w and inside domains d with rotating magnetization [4, 25, 31] (see Figure 1). Accurate calculations of the latter are impossible. We can however consider the motion and rotation induced Joule losses at a mesoscopic and then macroscopic scale. From a statistical resolution of the electromagnetic diffusion equations within the magnetic structure [25], it is well known that the power lost around each wall w and inside each domain d can be expressed as follow:

$$\iiint_{wall\ w} \sigma^{-1} j_{\mu w}^2 d^3r = \frac{2S_w}{\eta_w} v_w^2 = \frac{\sigma}{n_w}\left(\frac{n_w S_w J_s}{2\sigma\eta_w n_{wa}^2 A_w^2 (J_s^2 - J_\perp^2)}\left(\frac{\partial_t J_{//} - \frac{J_{//}.\partial_t\left(\sqrt{J_s^2-J_{s\perp}^2}\right)}{\sqrt{J_s^2-J_{s\perp}^2}}}{\partial_t B_{//}}\right)^2\right)\left(\partial_t B_{//}\right)^2 \tag{3}$$

$$\iiint_{domain\ d} \sigma^{-1} j_{\mu d}^2 d^3r = \frac{\sigma}{n_d} S_{DMR}\left(\partial_t\left(\sqrt{J_s^2 - J_{s\perp}^2}\right)\right)^2 = \frac{\sigma}{n_d}\left(S_{DMR}\frac{J_s^2}{J_s^2 - J_{s\perp}^2}\left(\frac{\partial_t J_\perp}{\partial_t B_\perp}\right)^2\right)(\partial_t B_\perp)^2 \tag{4}$$

with $S_{DMR} = \frac{n_d}{4\pi}\iiint_d \iiint_d G(r', r)d^3r'd^3r$ (G is the Green kernel function, r gives the position within a microscopic reference frame).

$\boldsymbol{J_s}$, $\boldsymbol{J}$ and $\boldsymbol{B}$ are the saturation, average magnetic polarization and flux density in the material, $J_{s//}$, $J_{//}$ and $B_{//}$ are the components of $\boldsymbol{J_s}$, $\boldsymbol{J}$ and $\boldsymbol{B}$ parallel to the walls' direction, $J_{s\perp}$ and $J_\perp$ and are the components of $\boldsymbol{J_s}$ and $\boldsymbol{J}$ perpendicular to the walls' direction. σ is the electrical conductivity, n_w and n_d the volume walls and the domains density respectively, S_w is the walls' real but average surface, A_w its surface normal to its displacement direction, η_w its mobility. n_{wa} is the active walls density, *i.e.* the density of walls contributing to the flux density $\boldsymbol{B}$ variations. By using these parameters (S_{DMR}, n_w, S_w, n_{wa}, S_{wa}) and by including the magnetization components ($J_{s//}$, $J_{s\perp}$), it is now possible to consider various magnetization mechanisms such as the DWB, DWM, DWN, DWF… as 2nd order effects inside equations (3) and (4).

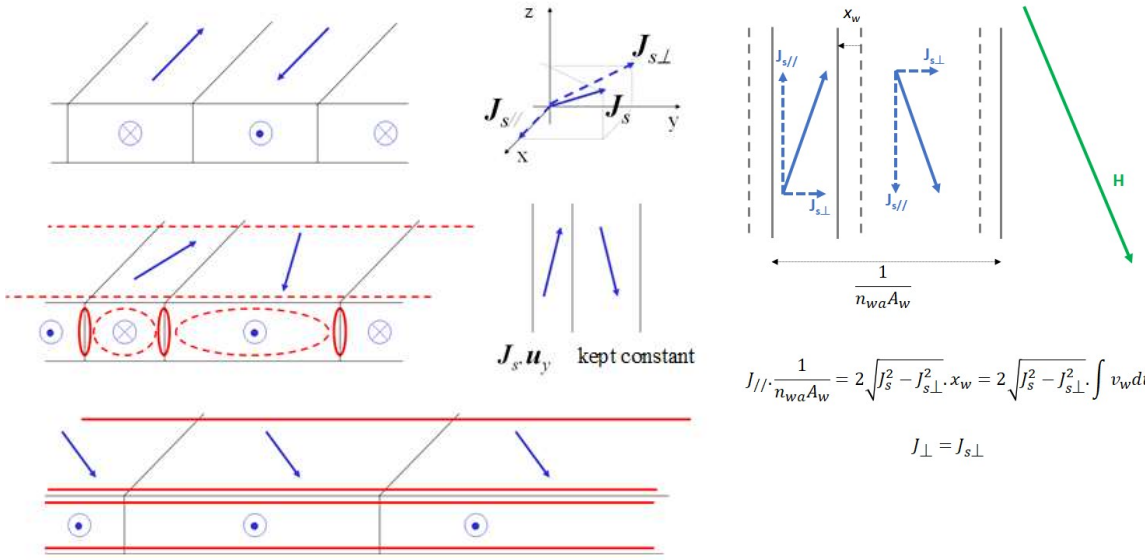

Figure 1: Magnetic structure, magnetization reversal mechanisms (DWD & DMR) and micro. eddy currents in a grain slightly misoriented with RD [25, 31].

2.1.2. Magnetic properties at the mesoscopic scale

The flux density derivative $\partial_t \boldsymbol{B}$ is created by the walls motion and the domains' magnetic rotation. Mechanisms are damped by anti-eddy fields $\boldsymbol{h}_{\mu w}$ and $\boldsymbol{h}_{\mu d}$ whose local integral parallel to $\partial_t \boldsymbol{B}$ can be determined, making equal Joule losses and magnetizing energies [26] (5):

$$\partial_t \boldsymbol{B}\iiint_w \boldsymbol{h}_{\mu w}(\boldsymbol{r})d^3r = \iiint_w \sigma^{-1}\boldsymbol{j}_{\mu w}^2(\boldsymbol{r})d^3r \text{ and } \partial_t \boldsymbol{B}\iiint_w \boldsymbol{h}_{\mu d}(\boldsymbol{r})d^3r = \iiint_d \sigma^{-1}\boldsymbol{j}_{\mu d}^2(\boldsymbol{r})d^3r \tag{5}$$

Accumulating microscopic energy located on each wall with surface S_w located at $\boldsymbol{r}_w$, or inside each domain of volume V_d located at $\boldsymbol{r}_d$, the total magnetic field $\boldsymbol{h}$ (see equation (6) and Figure 2) can be described with the sum of a quasi-static magnetic field $\boldsymbol{H}_M$ and two distribution functions (see equations (7) and (8))

$$\boldsymbol{h} = \boldsymbol{H}_M + \sum_w\left(\sigma\left[\Lambda_{DWD}^2\right]\partial_t\boldsymbol{B}\right)\frac{\Gamma(\boldsymbol{r}-\boldsymbol{r}_w, \boldsymbol{r}_w \in S_w)}{n_w S_w} + \sum_d\left(\sigma\left[\Lambda_{DMR}^2\right]\partial_t\boldsymbol{B}\right)\frac{\Theta(\boldsymbol{r}-\boldsymbol{r}_d, \boldsymbol{r}_d \in V_d)}{n_d V_d} \tag{6}$$

$$\iiint \Gamma(\boldsymbol{r}-\boldsymbol{r}_w, \boldsymbol{r}_w \in S_w)d^3r = S_w;\ \forall \boldsymbol{g}, \iiint \boldsymbol{g}(\boldsymbol{r})\Gamma(\boldsymbol{r}-\boldsymbol{r}_w, \boldsymbol{r}_w \in S_w)d^3r = \iint_{S_w}\boldsymbol{g}(\boldsymbol{r}_w)d^2r_w \tag{7}$$

$$\iiint \Theta(\boldsymbol{r}-\boldsymbol{r}_d, \boldsymbol{r}_d \in V_d)d^3r = V_d;\ \forall \boldsymbol{f}, \iiint \boldsymbol{f}(\boldsymbol{r})\Theta(\boldsymbol{r}-\boldsymbol{r}_d, \boldsymbol{r}_d \in V_d)d^3r = \iiint_{V_d}\boldsymbol{f}(\boldsymbol{r_d})d^3r_d \tag{8}$$

Λ_{DWD} and Λ_{DMR} are homogenized structural properties associated to the first order mechanisms [25] named the **D**omains' **W**all **D**isplacement (DWD, (9)) and the **D**omains' **M**agnetization **R**otation (DMR, (10)). Their limits study can be found in *Appendix 1*.

$$\Lambda_{DWD} = \sqrt{\frac{n_w S_w J_S}{2\sigma\eta_w n_w^2 a A_w^2 (J_S^2 - J_{S\perp}^2)}} \left(\frac{\partial_t J_{//} - \frac{J_{//}\partial_t\left(\sqrt{J_S^2 - J_{S\perp}^2}\right)}{\sqrt{J_S^2 - J_{S\perp}^2}}}{\partial_t B_{//}} \right) \tag{9}$$

$$\Lambda_{DMR} = \sqrt{S_{DMR}\frac{J_S^2}{J_S^2 - J_{S\perp}^2}} \left(\frac{\partial_t J_\perp}{\partial_t B_\perp} \right) \tag{10}$$

The quasi static magnetic field $\boldsymbol{H_M}$, responsible for the an hysteretic magnetization at equilibrium, is mainly driven by the sum of the magneto-crystalline anisotropy field, the local demagnetizing or shape anisotropy field and the residual stress induced anisotropy field. Microscopic anti eddy fields are mainly induced by eddy currents within the magnetic structure and are always quite smaller than the quasi static magnetic field $\boldsymbol{H_M}$ but responsible for the magnetic losses. Estimating the losses forbids to neglect those anti-eddy fields. For Fields $H_M < 25$ A.m^{-1}, *i.e.* for induction levels $B < 1.25$ T, the anti eddy field due to the DMR mechanism is negligible in front of the anti eddy field due to the DWD mechanism. In references [25, 31] for example, comparison is made between the characteristic time constants: τ_{DWD} due to DWD and τ_{DMR} due to DMR: $\frac{\tau_{DWD}}{\tau_{DMR}} = \left(\frac{\Lambda_{DWD}}{\sqrt{S_{DMR}}}\right)^2$. Below saturation: $\frac{\tau_{DWD}}{\tau_{DMR}} = \left(\frac{\Lambda_{DWD}}{\sqrt{S_{DMR}}}\right)^2 \approx \left(\frac{200}{20}\right)^2 = 100$, in the presence of enough walls, we effectively have no influence of the DMR process. However, above the knee point of magnetization curve with $H_M >$ 25 A.m^{-1} and $B > 1.25$ T: $\frac{\tau_{DWD}}{\tau_{DMR}} = \left(\frac{\Lambda_{DWD}}{\sqrt{S_{DMR}}}\right)^2 < \left(\frac{50}{20}\right)^2 = 6$, Λ_{DWD} decreases and tends towards a value which is comparable to the value of S_{DMR} (which might increases due to an increase of the domains size, with a limit which might correspond to the grain size). There will be a limit found for $(\Lambda_{DWD} + \Lambda_{DMR})$ at high frequency whatever the induction level which doesn't tend towards 0, so it is suggested that this non nil limit value is partly due to Λ_{DMR}, related to slightly but always misoriented grains and domains. The latter should allow not only to include the effect of magnetization rotation but more generally the effect of "classical-like" microscopic eddy currents with typical conduction length associated to the width and the length of domains within a grains.

Domains and walls may not be all parallel to one direction, even in a GOES. Thus, an averaging technique is proposed to take the various possible orientations into account (see Figure 2). Then, we define the rotation tensor $[\varpi(\theta_w)]$ to consider the projection $\partial_t \boldsymbol{B}$ along each wall and domain (see Figure 2 and equation (11)). $\overrightarrow{\theta_w}$ is a unit vector parallel to the wall's direction. $[\varpi(\theta_w)]$ is the tensor product of $\overrightarrow{\theta_w}$ with itself.

$$[\varpi(\theta_w)] = \overrightarrow{\theta_w} \otimes \overrightarrow{\theta_w} = \overrightarrow{\theta_w} \cdot \overrightarrow{\theta_w}^t = \begin{bmatrix} (\sin\theta_3 \cos\theta_{12})^2 & (\sin\theta_3)^2 \cos\theta_{12} \sin\theta_{12} & \cos\theta_3 \sin\theta_3 \cos\theta_{12} \\ (\sin\theta_3)^2 \cos\theta_{12} \sin\theta_{12} & (\sin\theta_3 \sin\theta_{12})^2 & \cos\theta_3 \sin\theta_3 \sin\theta_{12} \\ \cos\theta_3 \sin\theta_3 \cos\theta_{12} & \cos\theta_3 \sin\theta_3 \sin\theta_{12} & (\cos\theta_3)^2 \end{bmatrix} \tag{11}$$

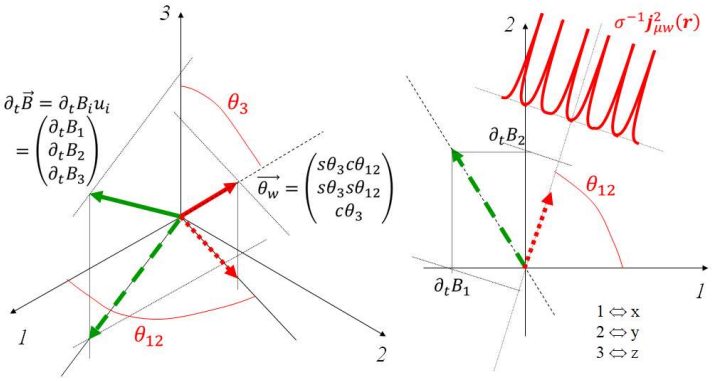

Figure 2: Definition of the whole possible domain walls orientation angle θ_w. $\overrightarrow{\theta_w}$ is a unit vector parallel to the wall's direction. Each oriented wall w may induce eddy current losses $\sigma^{-1}\boldsymbol{j}_{\mu w}^2(\boldsymbol{r})$ that will depend on θ_w in addition to the walls' density n_w, mobility η_w and surface S_w mentioned previously.

Then we choose to define the homogenized tensors $[\Lambda_{DWD}^2]$ and $[\Lambda_{DMR}^2]$ averaged over the whole possible directions $\boldsymbol{\theta}_w$ of walls and domains (equations (12) and (13)). Of course for a GOES, diagonal components of previous tensors in the rolling direction will be much higher than non diagonal contributions and than in the other directions. However, as mentioned above, it is suggested to keep the consideration of both $[\Lambda_{DWD}^2]$ and $[\Lambda_{DMR}^2]$ even in GOES especially at high induction or high frequency levels.

$$\left[\Lambda_{DWD}^2\right] = \frac{1}{2}\overline{n_w} \iint \frac{\Lambda_{DWD}^2(\theta_w)}{n_w(\theta_w)} [\varpi(\theta_w)] d\theta_3 d\theta_{12} \,;\, \overline{n_w} = \frac{1}{2\pi^2} \iint n_w(\theta_w) d\theta_3 d\theta_{12} \tag{12}$$

$$\left[\Lambda_{DMR}^2\right] = \frac{1}{2}\overline{n_w} \iint \frac{\Lambda_{DMR}^2(\theta_w)}{n_w(\theta_w)} ([1] - [\varpi(\theta_w)]) d\theta_3 d\theta_{12} \,;\, \overline{n_w} = \frac{1}{2\pi^2} \iint n_w(\theta_w) d\theta_3 d\theta_{12} \tag{13}$$

2.1.3. Static hysteresis behavioral law

In the following for GOES, the behaviour can be considered very simply with one scalar component $\Lambda^2 = \Lambda_{xx}{}^2$.

The static hysteresis loss contribution is not taken into account in a strict sense in this paper but can be included in the present model if required (solutions given in the references [17, 25, 32]). As a consequence, the whole possible hysteresis, especially with minor loops at very low frequencies, cannot be predicted faithfully except if we develop the present model by including a model of static hysteresis. The reasons for this choice to put aside the static hysteresis are as follow:

- In accordance with the title of the paper and the abstract; the aim of the paper is not to have a fine prediction of the hysteresis in the whole possible working conditions, except maybe at low and medium frequencies and high enough frequencies, *i.e.* frequencies for which the non linear properties μ and Λ shall be sufficient to reproduce faithfully the major loops of hysteresis and the total losses.
- Adding the static hysteresis model to this formulation is of course possible but it adds a complexity which is not useful to prove the main conclusions proposed by this contribution: In fact, as for the quasi-static magnetization curve and permeability (see Figure 14), the shape and area of the quasi static hysteresis loops does not depend significantly on the thickness of the material in hand but rather on its grains boundaries density (similar for the four thicknesses tested in this paper and in [34]). Therefore, the conclusion that will follow in the present work shouldn't suffer from the absence of a static hysteresis model. It will be the same if we add the static hysteresis model with the same relative differences but smaller absolute values of Λ, only for frequencies below 50 Hz.
- If we put aside the problems of memory effects and minor loops, the origin of static losses can be found within microscopic eddy currents induced during the stochastic jumps of walls from one defect to another (physically, theses jumps can be considered as equivalent dynamic effects that stay even with very very low variations). The separate identification of this effect can be done only at very low frequencies, because even at low frequency; and at the frequency for which we started our frequency dependent study (30Hz), the pure static effects of jumps are mixed with significant dynamic reversal effects related to the natural domains walls displacement, as the ones lumped in Λ (9) through the three quantities: the walls density n_w, the walls surface S_w and the walls mobility η_w.

The μ - Λ model is compatible with the walls nucleation, bowing, multiplication and dissipative motions from one defect to another only if we are not interested in the memory effects and minor loops. Then it is possible to reproduce the major hysteresis loops and losses above 30 Hz by having a property Λ which includes the static contribution (so which is overestimated but the same way for every thicknesses). In this case, the property Λ would be in the form:

$$\Lambda = \Lambda_{TOTAL} = \sqrt{\Lambda_{stat}^2 + \Lambda_{dyn}^2} \quad \text{with } \Lambda_{stat}(B,\omega) \approx \sqrt{\frac{\nu_c(B)}{\sigma\omega}} \underset{\omega\gg}{\longrightarrow} 0 \tag{14}$$

such that $j\sigma\Lambda_{stat}^2\omega \approx j\,\nu_c$ with $H_c \approx \nu_c B$ and $H_c B \propto \nu_c B^2$ is the quasi-static hysteresis energy loss per cycle. Λ_{stat} is the part of Λ which is exclusively linked to the quasi-static magnetization reversal mechanisms, meaning that one expression of the coercive field would be then as follows:

$$H_c \underset{\omega\ll}{\approx} 2\left(\frac{\omega}{\eta_{wa,static}(\omega)n_{w,static}(\omega)S_{w,static}(\omega)}\right).\frac{B}{J_s} \text{ with } \eta_{wa,static}(\omega)n_{w,static}(\omega)S_{w,static}(\omega) \underset{\omega\ll}{\approx} \frac{\omega}{\nu_c} \tag{15}$$

The development of a static hysteresis model included in the μ - Λ model this way and able to rebuild with even more accuracy the whole hysteresis loops presented in Figure 20 would be the subject of another dedicated contribution. In fact, for very low frequencies below 10-30 Hz, Λ becomes too high and we must separate the quasi static and dynamic losses and put in Λ only Λ_{dyn} which is linked exclusively to the dynamic magnetization reversal mechanisms. Otherwise, no conclusion can be guaranteed for low frequencies below 30 Hz, and the main conclusions must concern frequencies between 50 and 800 Hz, frequencies for which giving more importance to the dynamic losses in front of static losses usually makes sense.

2.1.4. Dynamic hysteresis behavioral law

Smoothing and averaging equation (16), thanks to specific functions slowly varying in space ([25] and Figure 2), we can express a smooth mesoscopic but total magnetic field $\boldsymbol{H}$ influenced by the dynamic damping contribution [26]:

$$\boldsymbol{H} = \boldsymbol{H}_M(\boldsymbol{B}) + \sigma\left[\Lambda^2\right](\boldsymbol{B},\partial_t\boldsymbol{B})\partial_t\boldsymbol{B} \tag{16}$$

$$\left[\Lambda^2\right] = \left[\Lambda_{DWD}^2\right] + \left[\Lambda_{DMR}^2\right] \tag{17}$$

$\boldsymbol{H}_M$ is defined as the quasi-static magnetic field without static hysteresis which is not detailed in this paper. $[\Lambda^2]$ is the homogenized structural parameter called dynamic magnetization property. In the following for GOES, the dynamic behavior can be considered very simply with one scalar $\Lambda^2 = \Lambda_{xx}^2$. The DWD mechanism is firstly invoked as the main contribution for GO sheets for most working conditions. However the DMR mechanism is kept as one contribution to the magnetization reversal mechanisms with importance that depends on the induction and frequency levels. This importance that increases with the induction and frequency levels is closely linked to the following specificities of an electrical steel and of a GOES:

- Grains of GOES are not perfectly oriented in the same rolling direction but can be oriented with an angle either in plane or out of plane that can be from -7 to +7° in average.
- Grains of GOES are abnormally big but they have got a finite size from 15 to 30 mm in average.

As a consequence, when the whole walls of a grain disappear, there is still the last DMR process that allows to keep the magnetization models consistent: If the DMR is not taken into account close to saturation, the theoretical value of the magnetic properties become inconsistent with divergence which is physically impossible or with nil value which is not experimentally observed (see *Appendix 1*). Taking the DMR into account close to saturation helps describing classical-like loss contributions related to "classical" microscopic eddy currents with typical conduction length associated to the width and the length of domains within the lasting and non perfectly oriented grains … This contribution is included in the present model through the contribution of domains geometrical parameter S_{DMR} inside the property Λ and through the field equations that follow. Thus the next step is to include static and dynamic magnetization properties within a field diffusion-like equation that can be derived from the Maxwell equations.

2.2. Field diffusion with magnetization mechanisms

2.2.1. Field diffusion-like equation

Assuming static properties $\boldsymbol{B} = \mu(H_M)\boldsymbol{H}_M$ and $d\boldsymbol{B} = \mu_d(H_M)d\boldsymbol{H}_M$ (μ is called the internal static permeability and μ_d is the static differential permeability), the Ohm law and the Maxwell formulae; the field diffusion-like equation in a macroscopic reference frame becomes:

$$curl\left(\sigma^{-1}curl\left(\left(1+\sigma\left[\Lambda^2(\boldsymbol{H}_M,\partial_t\boldsymbol{H}_M)\right]\mu_d(\boldsymbol{H}_M)\partial_t.\right)\boldsymbol{H}_M\right)\right)+\mu_d(\boldsymbol{H}_M)\partial_t\boldsymbol{H}_M=0 \quad (20)$$

$$\mu_d(\boldsymbol{H}_M)=\mu(\boldsymbol{H}_M)+\partial_{H_M}\mu(\boldsymbol{H}_M).\boldsymbol{H}_M \quad (21)$$

The interest of such a mesoscopic description is that it includes an average dynamic property $[\Lambda^2]$ that represents the magnetic structure with domains and walls and that the computation of dynamic losses and hysteresis becomes compatible with Finite Element formulations. It is important now to identify the property $[\Lambda^2]$ and check the relevance of such a description. The main problem of such a representation, close to references [23, 26], is that it is very hard to foresee and separate actual microscopic structures. It is for example not possible to discriminate between an effect of domains refinement (n_w), walls activation (n_{wa}), an increase of the walls surface (S_w and A_w) or mobility (η_w) or a simultaneous contribution of the domains' magnetization rotation (S_{DMR}).

Let's study a standard 30*300 mm laminated electrical steel sheet with GO SiFe adapted to the Epstein Frame. Let's assume that this problem is 1D (One Dimensional) and one-directional, *i.e.* the magnetic field $\boldsymbol{H}_M = H_M.\boldsymbol{u}_x$ and induction $\boldsymbol{B} = B.\boldsymbol{u}_x$ are in one direction x and they depend only on one other direction z (See Figure 3). By considering for the dynamic behaviour one scalar $\Lambda^2 = \Lambda_{xx}^2$, the Partial Differential Equation (20) becomes (22) in 1D with a one-directional magnetic field:

$$\partial_z^2\left(\left(1+\sigma\Lambda^2(H_M,\partial_tH_M)\mu_d(H_M)\partial_t.\right)H_M\right)-\mu_d(H_M)\partial_tH_M=0 \quad (22)$$

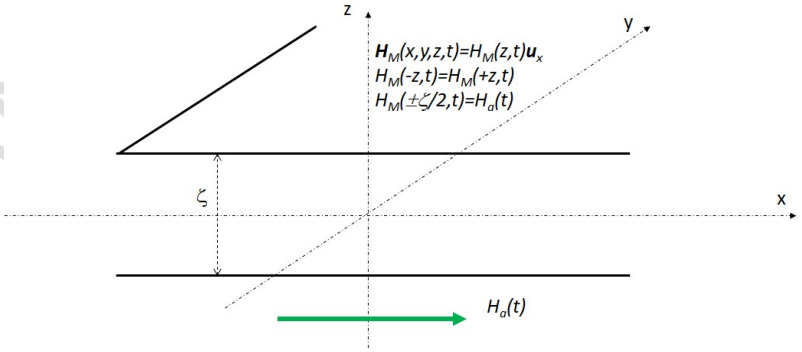

Figure 3: 1D geometry of the test case studied – an electrical steel sheet with one directional field.

2.2.2. Calculations at low induction

At low induction, we consider that every parameter $(\sigma,\mu=\mu_d,\Lambda)$ is a constant, meaning that the problem is linear and can be solved with complex variables. In this case, we can assume the magneto harmonic conditions and the partial differential equation (22) leads to the wave vector like dispersion equation (23)

$$\left(1+j\sigma\Lambda^2\mu\omega\right)k^2+j\sigma\mu\omega=0 \quad (23)$$

ω is the angle velocity of harmonic flux variations and $j=e^{j\pi/2}$ is the pure imaginary complex number.

Equation (23) has got a well-known solution (25) [26] that uses two complementary wave vectors defined by (24).

$$k_\pm=\sqrt{\frac{1}{2}\left(\frac{\sigma\mu\omega}{1+(\sigma\Lambda^2\mu\omega)^2}\right)}\sqrt{\pm\sigma\Lambda^2\mu\omega+\sqrt{1+\left(\sigma\Lambda^2\mu\omega\right)^2}} \quad (24)$$

$$H_M(z,t)=\tilde{H}_M(z)e^{j\omega t}=\frac{H_a}{(1+j\sigma\Lambda^2\mu\omega)}\frac{\cosh(j(k_--jk_+)z)}{\cosh(j(k_--jk_+)\zeta/2)}e^{j\omega t} \quad (25)$$

The skin effect is thus modified by Λ in depth but also in phase angle [26].

2.2.2.1. Magnitude and apparent permeability

Thus, it is now possible to calculate the magnitude magnetic permeability defined by the ratio between the flux density and the magnetic field applied at the material surface named H_a given in (26):

$$\underline{\mu}_{mag}(\mu,\Lambda,\omega)=\frac{\tilde{B}}{H_a}=\frac{\frac{1}{\zeta}\int_{-\zeta/2}^{+\zeta/2}\mu\tilde{H}_M(z)dz}{H_a}=\frac{2\mu\tan\left((k_++ik_-)\zeta/2\right)}{\zeta(1+i\sigma\Lambda^2\mu\omega)(k_++ik_-)}=\mu_{mag}e^{j\varphi_{mag}} \quad (26)$$

In the following, we will also need to use the apparent magnetic permeability defined with the peak induction $B=\left|\tilde{B}\right|$ by (27).

$$\mu_{app}(\mu,\Lambda,\omega)=\frac{B}{H_a\cos(-\varphi_{mag})}=\frac{\mu_{mag}}{\cos(-\varphi_{mag})} \quad (27)$$

Both μ_{mag} and μ_{app} depend on σ, μ and Λ. Assuming that the electrical conductivity σ is known ($\sigma^{-1} = \rho = 48\ \mu\Omega.cm$ for the GO SiFe studied), it is necessary to get a second information measured in order to identify the two last unknown properties μ and Λ. Nevertheless, the apparent permeability at very low frequency $\mu_{app}(\mu, \omega \to 0)$ allows us to identify μ separately from Λ. Then both the apparent permeability and the total losses allow us to identify the dynamic property Λ as a function of the induction B and the frequency f. However, since the experimental error is higher for the apparent permeability, we decide to identify the dynamic property Λ thanks to the magnetic losses. Figure 4 and Figure 5 show the relative apparent magnetic permeability $\mu_{app,r}=\mu_{app}/\mu_0$ measured at low induction levels for four thicknesses of one GO SiFe measured on Epstein strips as a function of the spatial average induction level B and the frequency f (see § 3.2). The whole experimental errors analysis can be found in *Appendix 2* at the end of this paper. As expected, these permeabilities increase with the flux density due to the usual first magnetization curve at low induction but decrease with the frequency due to the magnetic field damping related to macroscopic and microscopic eddy currents. At the same time, the apparent permeability decreases when the electrical sheet thickness increases. In fact, anti-eddy fields increase for sheets thicker than the modified skin depth.

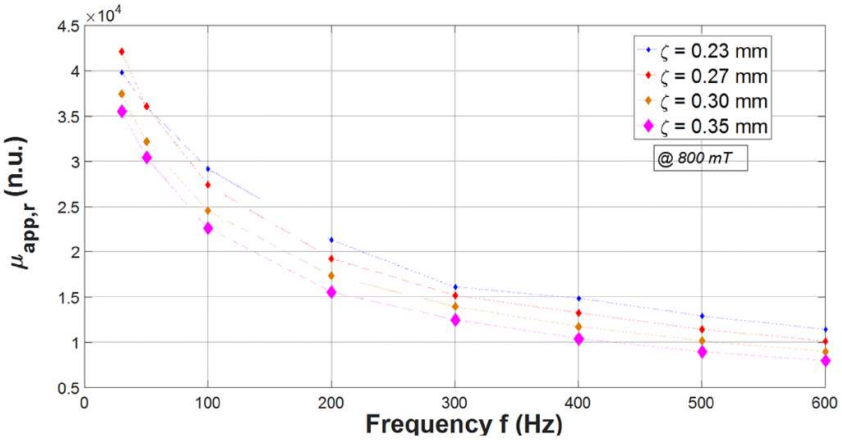

Figure 4: Measurement of the relative apparent magnetic permeability $\mu_{app,r}$ as a function of the average flux density level B @ f = 600 *Hz*. Experimental errors for $\mu_{app,r}$ can be found in the *Appendix 2* ($\delta(f\ \mu_{app}/\mu_0) = \left(\pm 3240 \pm 3\%(f\ \mu_{app}/\mu_0)\right)$ [*Hz*]).

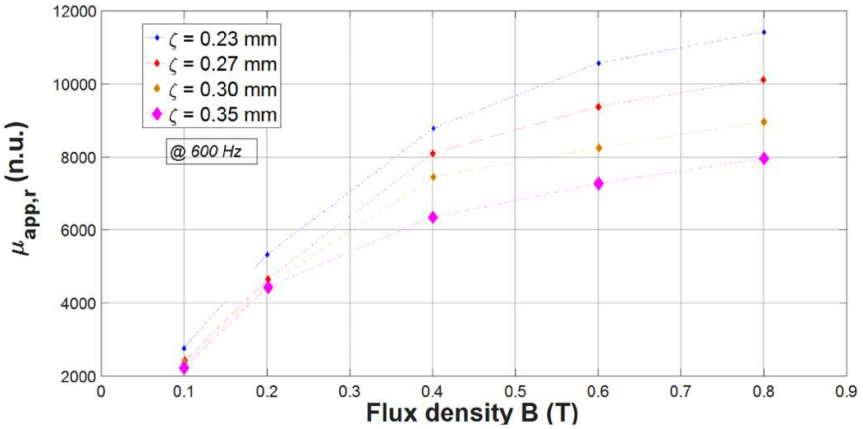

Figure 5: Measurement of the relative apparent magnetic permeability as a function of the frequency f @ B = 800 *mT*. Experimental errors for $\mu_{app,r}$ can be found in the *Appendix 2* ($\delta(f\ \mu_{app}/\mu_0) = \left(\pm 3240 \pm 3\%(f\ \mu_{app}/\mu_0)\right)$ [*Hz*]).

2.2.2.2. Iron losses

It is also possible to calculate the total magnetic losses defined either by the magnetic energy or the electrical energy given in (28):

$$E_{mf}(\mu, \Lambda, \omega) = \frac{\pi}{\gamma} Re\left(jH_a \frac{1}{\zeta}\int_{-\zeta/2}^{+\zeta/2} \mu \tilde{H}_M(z)dz\right) = \frac{1}{2f\gamma} Re\left(\frac{1}{\zeta}\int_{-\zeta/2}^{+\zeta/2} \rho\left|\nabla \times \tilde{H}(z)\right|^2 dz\right)$$

$$= \frac{\pi\zeta B^2}{2\mu\gamma}\left(\frac{cosh(\zeta k_+) + co\ (\zeta k_-)}{sinh^2(\zeta k_+) + s\ ^2(\zeta k_-)}\right)\begin{pmatrix}\left(\sigma\Lambda^2\mu\omega k_+ + k_-\right) sinh(\zeta k_+) + \\ \left(\sigma\Lambda^2\mu\omega k_- - k_+\right) sin(\zeta k_-)\end{pmatrix} \quad (28)$$

γ is the volume mass density. Figure 6 shows the total average energy loss density E_{mf} per unit mass measured per cycle at low induction levels for four thicknesses of one GO SiFe measured on Epstein strips as a function of the spatial average induction level B and the frequency f (see § 3.2). The whole experimental errors analysis can be found in *Appendix 2* at the end of this paper. As expected, the losses increase with the flux density and with the frequency due to DWD and DMR microscopic eddy currents. At the same time, the losses increase when the electrical sheet thickness increases. In fact, eddy current losses become more important for thickness bigger than the modified skin depth.

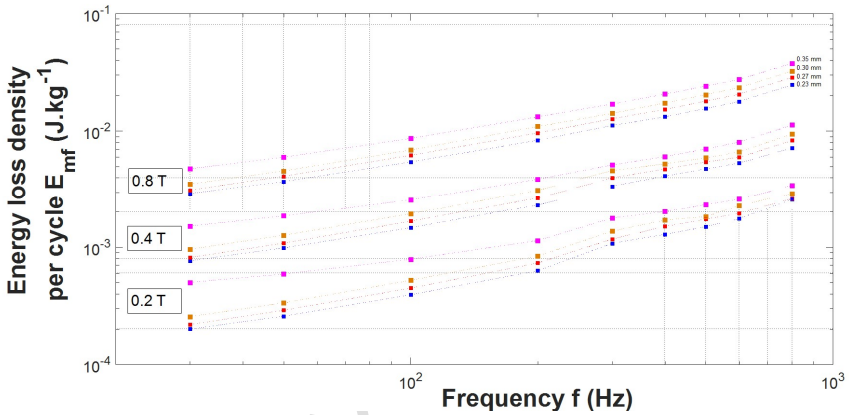

Figure 6: Measurement of the total magnetic losses as a function of the average induction B and the frequency f.
Experimental errors for an energy loss density E_{mf} can be found in the *Appendix 2* ($\delta(fE_{mf}) = \left(\pm 0.26 \pm 3\%(fE_{mf})\right)[mW/kg]$).

2.2.3. Calculations at high induction

2.2.3.1. Magnetic dynamic hysteresis

At higher induction levels, due to non-linear relationships between the magnetic field H or H_M and the flux density B, calculating the apparent permeability or/and the losses is possible only if accurate hysteresis loops can be reproduced. Each loci of any cycle can be calculated step after step by solving (22) time after time numerically (the Finite Difference Method for example). In the hysteresis loops simulations, there are two steps:

(i) In the first step called identification step presented here in § 3, the parameter $\Lambda(B, \partial_t B)$ or $\Lambda(H_M, \partial_t H_M)$ is varied and sought until the calculation gives the same point (t, H, B) within each cycle measured at various frequencies, providing the accuracy required is specified. This step needs an iterative procedure that takes time inversely proportional to the accuracy.

(ii) In the second step called computation step presented in § 4, each cycle is rebuilt by using a fitting model for $\Lambda(H_M, \partial_t H_M)$. This step allows direct computations without iterations but keeps some inaccuracies related to the fitting model used.

Figure 7 shows the hysteresis loops measured at higher induction levels for four thicknesses of one GO SiFe measured on Epstein strips as a function of the spatial average induction level B and the frequency f. The whole experimental errors analysis can be found in *Appendix 2*. As expected, the hysteresis loops area increases with the frequency because of the losses (see (28) and next §). Figure 7 also shows the hysteresis loops rebuilt by identifications for the same experimental conditions, *i.e.* by adjusting the properties $\mu(H_M)$ and $\Lambda(H_M, \partial_t H_M)$ inside the model, in order to minimize the discrepancies between the measurements and the calculations done for identifications.

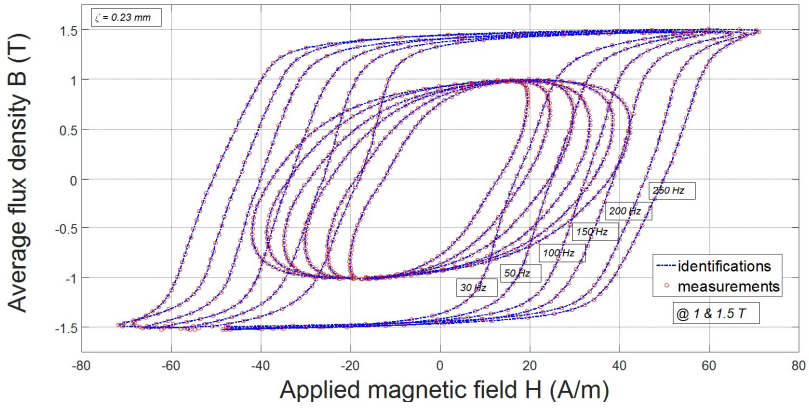

Figure 7: Measurement and identification calculation of hysteresis cycles between the spatial average of B and the total surface magnetic field applied $H=H_a$.
Experimental errors for H and B can be found in the *Appendix 2* ($\delta H = (\pm 1.5 \pm 2\%H)[A/m]$ and $\delta(fB) = \left(\pm 0.21 \pm 2\%(fB)\right)[T.Hz]$).

2.2.3.2. Magnetic losses

Once the hysteresis loops are measured or/and computed, then the magnetic losses can be calculated as follows (29)

$$E_{mf}(\mu, \Lambda, \omega) = \frac{1}{\gamma}\int_{-1/(2f)}^{1/(2f)} \left(H_a(t)\frac{1}{\zeta}\int_{-\zeta/2}^{+\zeta/2}\left(\mu\tilde{H}_M(z,t)\right)dz\right)dt \qquad (29)$$

It can be shown that the total magnetic losses, *i.e.* the total eddy currents losses, correspond to the total area inside each cycle [25].

At the end, the loss predicting ability of this model can be considered if and only if it is tested and extensively checked by measuring a substantial number of hysteresis loops (up to 50 cycles per thickness and 200 in total, with 1000 data points per cycles that makes 50°000 data points per thickness and up to 200 000 data points to be analyzed and post-treated, see Figure 15 and Figure 16). Then, the model

parameters can be determined with one consistent and complex identification procedure including linear and non linear steps. However the calculation time stays reasonable: approximately half a day, data processing included. The next section gives the results found on fours different GOES samples with four different thicknesses. The list of samples used and the experimental set-up and its accuracy will be described. Then, the static internal permeability μ and the dynamic magnetization property Λ are identified within both linear and non linear assumptions as a function of B and f ($\mu(B)$ and $\Lambda(B,f)$) or H_M and $\partial_t H_M$ ($\mu(H_M)$ and $\Lambda(H_M,\partial_t H_M)$) respectively.

3. Identification and interpretation of mesoscopic properties

3.1. The samples

In the following, we propose to analyze the magnetic loss and behavior of one GO SiFe steel (@TKES*) laminated with four different thicknesses. The whole specimens are manufactured with the same initial chemical composition (SiFe with 3% of Si), the same recrystallisation process and the same coating process. Epstein samples (with dimensions 30*300 mm^2) with a stress releasing annealing after cutting were used. Measurements were carried out on four thicknesses (ζ = 0.23 / 0.27 / 0.30 / 0.35 *mm*). The volume mass density of this GO steel is γ=7650 $kg.m^{-3}$ and its electrical resistivity ρ = 48 $\mu\Omega.cm$. The manufacturing processes are adapted for the whole samples in order to get anomalous large G.O.S.S. grains with no significant differences in terms of typical grains' dimension (20-40 *mm*), orientation (6° max disorientation), coating material (Inorganic based divided in two layers, one layer of glass-film and one layer of phosphated insulator) and coating thickness (2-4 μm) and its thermal curing temperature (T>~800°C, few minutes) (see § 5).

3.2. The experimental set-up – Epstein Frame

The experimental set-up used is the classical Epstein Frame with 700 windings and at least four 30*300 mm^2 samples, to form a closed magnetic circuit. This apparatus, designed for magnetic measurement of iron losses and the hysteresis, provides time dependent signals of the induction averaged in the thickness ($\tilde{B}(\omega)$ in the case of magneto-harmonic assumptions at low induction and $B(t)$ in the case of non-linear transient assumptions at higher induction) of the sheet versus the uniform surface magnetic field ($\widetilde{H_a}(\omega)$ in the case of magneto-harmonic assumptions at low induction and $H_a(t)$ in the case of non-linear transient assumptions at higher induction) by measuring respectively the voltage V in the secondary coils system and the current I in the primary coils. A time integral of V can give B thanks to the Faraday law. H_a is deduced from I thanks to the Ampere law. The user defines a specific induction signal (with an amplitude and a frequency) expected from the system and the magnetic field is generated in a way to respect the requested average induction. Estimation of the maximum inaccuracies mainly depend on the current I and voltage V measured:

$$\delta I = (\pm 2 \pm 1\% I)[mA];\ \delta V = (\pm 6.5 \pm 1\% V)[mV] \tag{30}$$

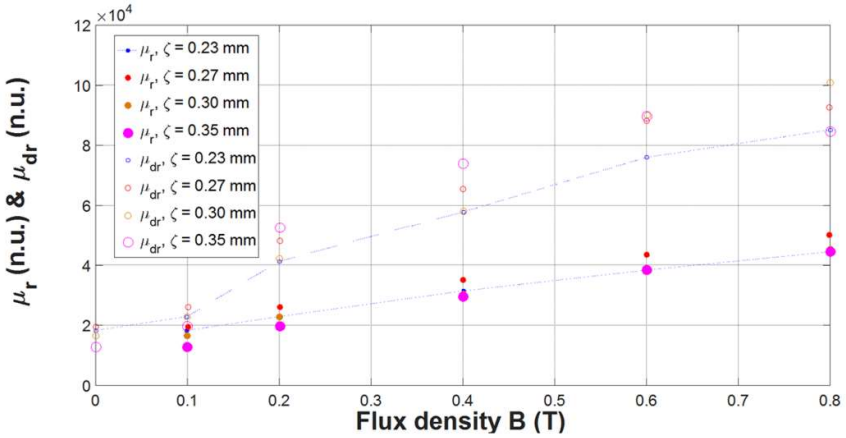

Figure 8: Measurement of the relative internal magnetic permeability μ_r as a function of the average flux density level B @ f = 10 *Hz*.
Experimental errors for μ_r can be found in the *Appendix 2* ($\delta(f\ \mu/\mu_0) = (\pm 3240 \pm 3\%(f\ \mu/\mu_0))[Hz]$).

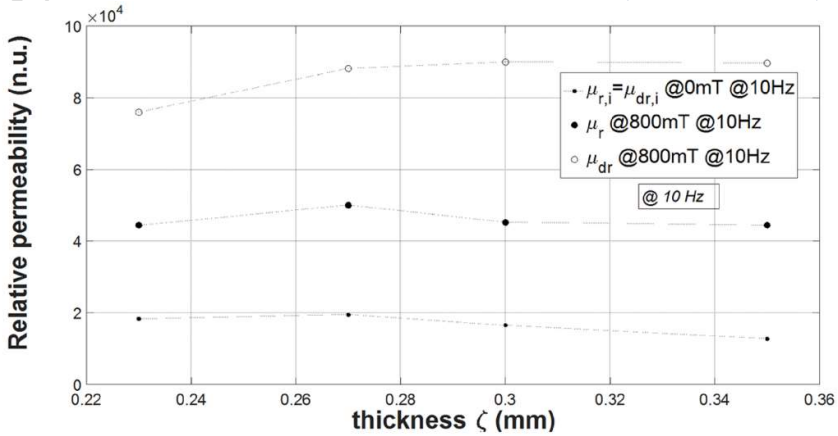

Figure 9: Measurement of the relative internal magnetic permeability μ_r as a function of the thickness ζ.
Experimental errors for μ_r can be found in the *Appendix 2* ($\delta(f\ \mu/\mu_0) = (\pm 2340 \pm 3\%(f\ \mu/\mu_0))[Hz]$).

3.3. Identification of mesoscopic properties

3.3.1. At low induction

3.3.1.1. The static magnetization property

As explained above, the internal magnetic permeability μ is identified by fitting the apparent permeability at very low frequency $\mu_{app}(\mu,\omega\rightarrow 0)$. The frequency f=10 *Hz* has been chosen, such that the skin depth is always higher than the biggest thickness 0.35 *mm*. Figure 8 gives the results obtained for the identification of μ and μ_d. The latter properties μ and μ_d depend mostly on the induction B but are neither significantly nor deterministically sensitive to the thickness ζ and this conclusion is confirmed in Figure 9.

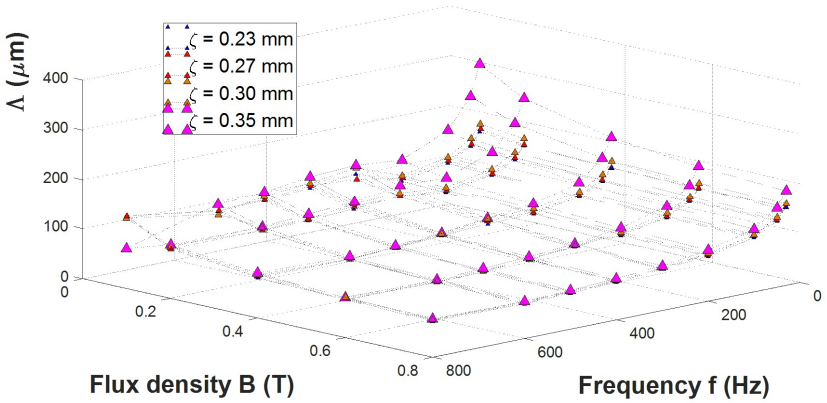

Figure 10: Experimental identification of the dynamic magnetization property Λ as a function of the induction B and the frequency f.
Experimental errors for Λ can be found in the *Appendix 2* ($\delta(fB\Lambda) = (\pm 6 \pm 1.5\%(fB\Lambda))[T.Hz.\mu m]$).

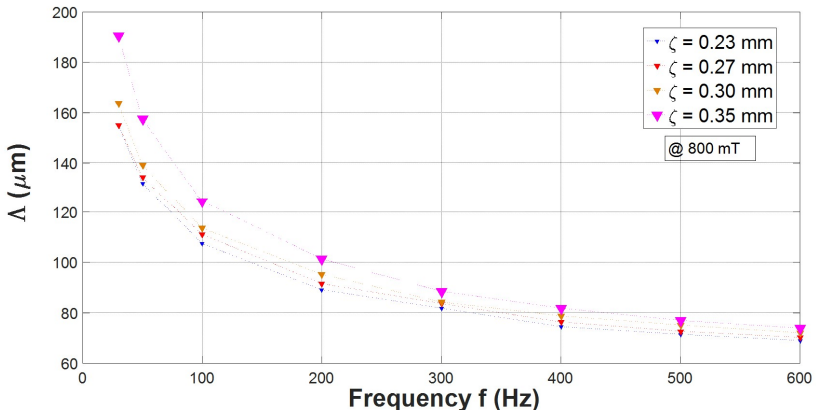

Figure 11: Experimental identification of the dynamic magnetization property Λ as a function of the induction B @ f = 600 *Hz*.
Experimental errors for Λ can be found in the *Appendix 2* ($\delta(fB\Lambda) = (\pm 6 \pm 1.5\%(fB\Lambda))[T.Hz.\mu m]$).

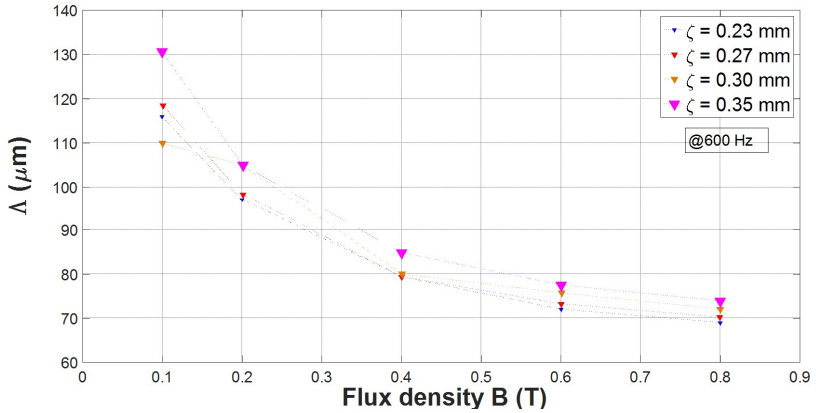

Figure 12: Experimental identification of the dynamic magnetization property Λ as a function of the frequency f @ B = 800 *mT*.
Experimental errors for Λ can be found in the *Appendix 2* ($\delta(fB\Lambda) = (\pm 6 \pm 1.5\%(fB\Lambda))[T.Hz.\mu m]$).

3.3.1.2. The dynamic magnetization property

The dynamic magnetization property Λ is identified by fitting the total magnetic losses for each induction level B and each frequency f. The whole experimental errors analysis can be found in *Appendix 2* at the end of this paper. Figure 10, Figure 11 and Figure 12 show the result of Λ identifications. The dynamic magnetization property decreases with both the induction B and the frequency f, probably due to second order phenomena such as the domain walls bowing, multiplication and nucleations. Close to saturation, the walls density tends towards 0 but the dynamic magnetization is still reduced and seems to tend towards a finite number. The reason for that might be the walls mobility that is greatly increased and the DMR mechanism for lasting small misoriented and closure domains that might contribute to Λ. The complete limits study can be found in *Appendix 1*. In any case, the model is exactly equivalent to the classical eddy currents model when $\Lambda \to 0$. Therefore, it seems that increasing enough the frequency and approaching more the saturation, we should tend towards this classical limit. When looking at the thickness ζ dependence of Λ then, we observe and confirm in Figure 13 that $\Lambda(\zeta)$ is an increasing function, probably due to the domains' refinement effect, the walls' surface reduction and the walls' mobility increase. If we consider that the stress releasing heat treatment does not modify the tensile stress exerted by the insulating coating onto the metal, then Lancet domains [29, 30] should be minimized and the main 180° domains refined due to surface magnetic poles created by the grains misorientation. The lower the thickness the finer the main 180° domains are in order to compensate an increase in the stray field energy from closer poles. If now we consider that Lancet domains are still present, the necessity for the material to create more Lancet domains appears for equivalent reasons. The problem is that the static permeability should be reduced at high induction due to high energy of magnetic poles in the first case, not necessarily in the second case. No significant decrease of the internal permeability as a function of the thickness ζ has been reported before. Therefore, we think that for the specimen received, there are still Lancet domains that do not absolutely optimize the losses but preserve the apparent permeability thanks to a compensation of the stray field energy of magnetic poles. This compensation can be obtained either by a refinement of main 180° domains or/and the multiplication of closure Lancet domains.

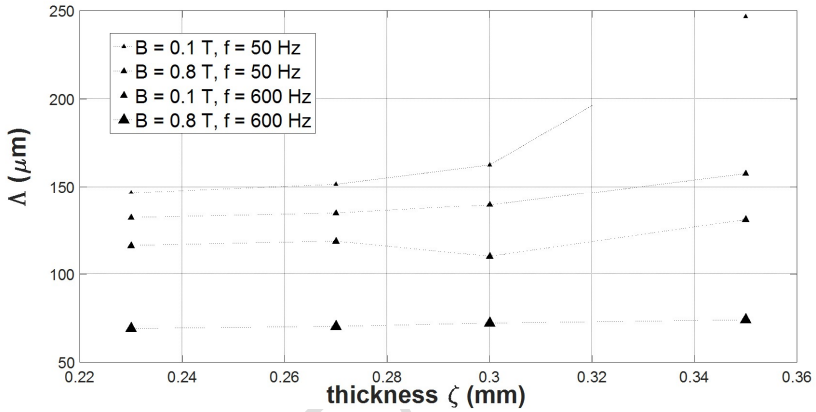

Figure 13: Experimental identification of the dynamic magnetization property Λ as a function of the thickness ζ
Experimental errors for Λ can be found in the *Appendix 2* ($\delta(fB\Lambda) = (\pm 6 \pm 1.5\%(fB\Lambda))[T.Hz.\mu m]$).

3.3.2. At high induction

3.3.2.1. The static magnetization properties

For non-linear case, the internal magnetic permeability can be identified the same way as in the case of linear case. The Figure 14 gives the data μ and μ_d determined by measurements of the first magnetization curve. The latter is necessary to reproduce hysteresis cycles at low induction with a constant internal permeability μ given by this curve for each loop. For higher induction levels with non-linear variations, it is necessary to have a model. In this case, it is proposed to use an anhysteretic curve model to define $\mu(H_M)$. In the whole cases and for the whole specimens, we can conclude that $\mu(H_M)$ depends mostly on the induction B but not on the thickness ζ. This conclusion is coherent with the previous linear results.

3.3.2.2. The dynamic magnetization property

In the non-linear case, the dynamic magnetization property Λ is identified by fitting the spatial average flux density B inside each loop. The whole experimental errors analysis can be found in *Appendix 2* at the end of this paper. Figure 15 gives $\Lambda(H_M=0,\partial_t H_M)$ coarse identifications for the whole measured data and the whole hysteresis. The results show lots of dispersion in the data that requires a smooth fitting function. Figure 15 shows the results using the fitting function (31) for which the parameters' values are listed in Table 1.

$$\Lambda = \Lambda_0 e^{-\frac{\left(\partial_t H_M + \frac{H_M}{\tau}\right)^2}{2\pi\epsilon_{dh}^2}} + \Lambda_l \tag{31}$$

The Gauss distribution of domains width and reversely of walls density [17, 25] seems adapted to describe an increasing population of walls due to walls multiplication and nucleation when the total dynamic field ($H_M + \tau\partial_t H_M$) is increasing too. ε_{dh} and $\tau\varepsilon_{dh}$ are threshold fields that lead to the standard deviation of the Gauss distribution of domains width versus the dynamic field and the total dynamic field respectively. When the fields magnitude goes up to these threshold fields, walls deformation, multiplication and nucleation start to occur making the dynamic magnetization property lower but non-linear. Λ_l is the minimum value of Λ achieved close to saturation, partly due to the physical limit achieved by Λ_{DWD} due to the DWD mechanism of lasting and isolated walls and partly due to the lasting contributions of the DMR mechanism in single domain grains slightly misoriented with the rolling direction (see *Appendix 1*).

One part of conclusions proposed in the linear case are still valid in the non-linear case. Figure 16 shows the equivalent results for $\Lambda(H_M, \partial_t H_M=0)$, which is approximately a constant. It seems logical that the dependence of Λ on H_M begins only when the field is varying in time ($\partial_t H_M \neq 0$). For both variations, Λ is a decreasing function which is coherent with the linear functions $\Lambda(B)$ and $\Lambda(f)$. However, the decrease as a function of B might be distorted compared to H_M due to the non-linear permeability μ. As expected and like within linear identifications in § 3.3.1.2, Table 1 shows that the parameter Λ tends towards Λ_0 for low induction and frequency, and that Λ_0 increases with the thickness ζ. On the contrary, the dynamic parameters ε_{dh} and τ decrease with the thickness ζ which means that mechanisms such as the walls nucleation, bowing or/and multiplication are relatively facilitated for higher thicknesses. As for the limit value Λ_l of Λ, related to DMR close to saturation, it seems to be minimized for the intermediate thickness 0.30 mm with a better grains' orientation.

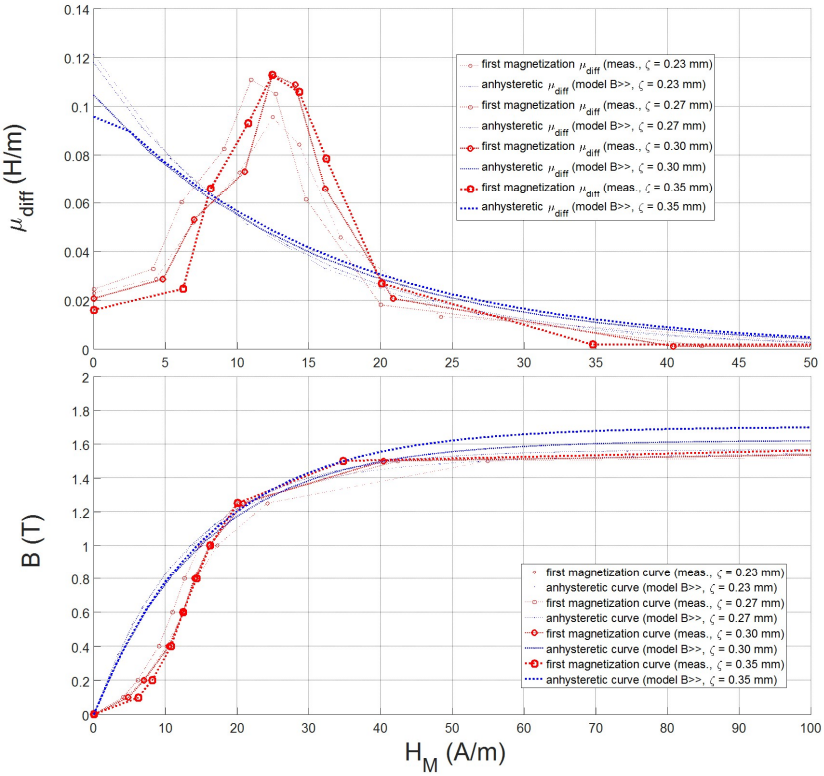

Figure 14: Measurement of the static magnetization curve $B(H_M)$ (---) and its corresponding differential permeability $\mu_d(H_M)$ (o). Experimental identification of a magnetization model for the static an hysteretic magnetization curve $B(H_M)$ (---) and its corresponding differential permeability $\mu_d(H_M)$ (o).

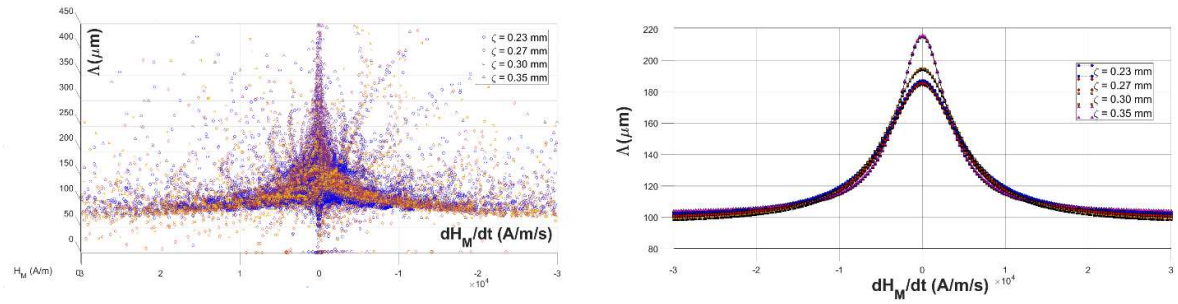

Figure 15: Experimental identification of $\Lambda(\partial_t H_M)$. Coarse measurements (left) and model (right).

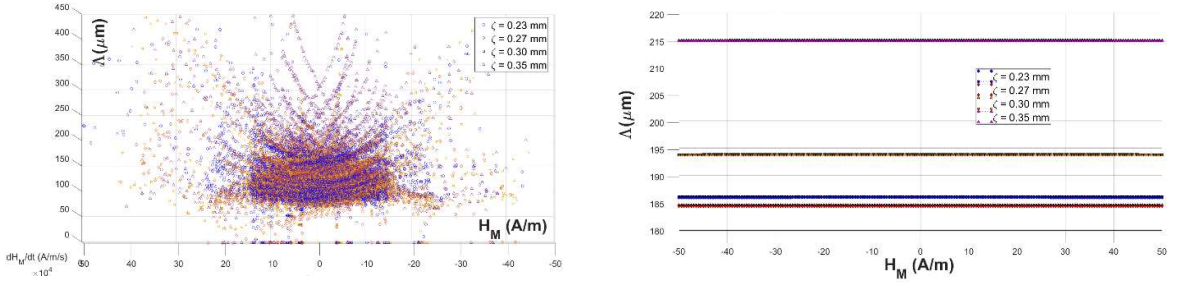

Figure 16: Experimental identification of $\Lambda(H_M)$. Coarse measurements (left) and model (right).

4. Computation of macroscopic magnetic properties

4.1. Presentation of global results at low induction

4.1.1. Hysteresis loops

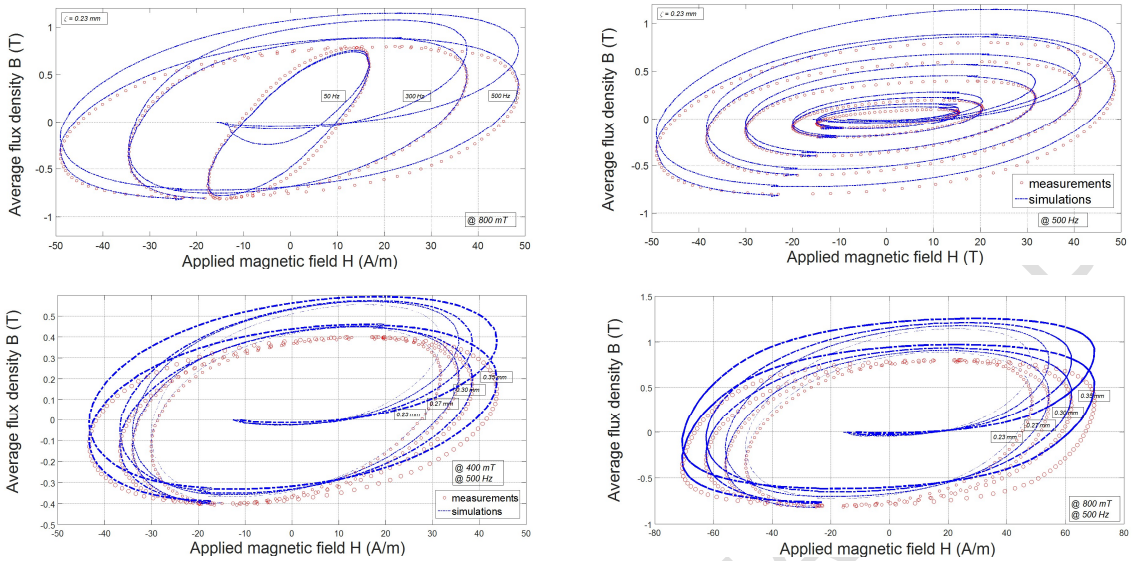

Figure 17: Measurement and computation of hysteresis cycles computed at low induction thanks to the model and μ and Λ identified experimentally. Experimental errors for H and B can be found in the *Appendix 2* ($\delta H = (\pm 1.5 \pm 2\%H)[A/m]$ and $\delta(fB) = (\pm 0.21 \pm 2\%(fB))[T.Hz]$).

Thanks to the accurate identification of μ and Λ, the hysteresis cycles can be accurately reproduced at low induction levels, i.e. with linear assumptions (see Figure 17). Significant discrepancies can be noticed for negative and intermediate flux densities up to 0.6 T; this might be due to a transient computation artefact. It should be possible to improve this by computing more periods and using an adequate non-linear property $\mu(H_M)$ even for these induction levels.

Table 1: material parameters identified for the dynamic magnetization property Λ

ζ [mm]	ε_{dh} [A.m^{-1}.s^{-1}]	τ [ms]	Λ_0 [μm]	Λ_l [μm]
0.23	5425	2.17	87.4	98.7
0.27	5290	2.25	87.3	97.2
0.30	5305	1.60	98.6	95.3
0.35	3590	1.55	113.5	101.5

4.1.2. Apparent magnetic permeability

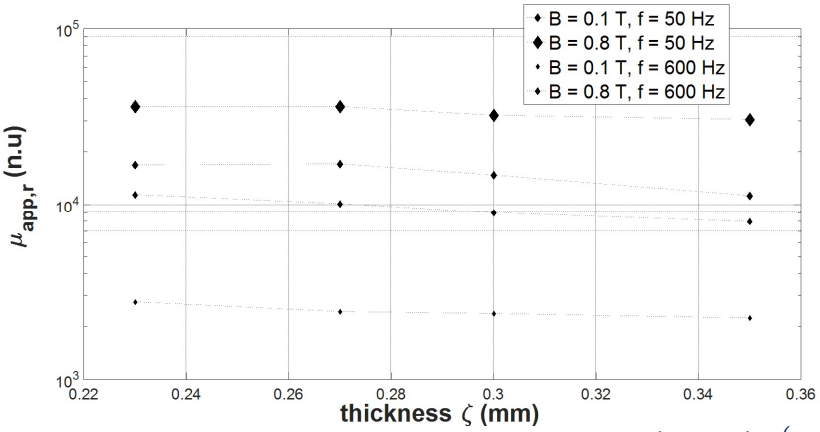

Figure 18: Measurement of relative apparent magnetic permeability ♦ as a function of the thickness ζ ($\delta(f\,\mu_{app}/\mu_0) = (\pm 3240 \pm 3\%(f\,\mu_{app}/\mu_0))\,[Hz]$).

Knowing the material properties, we can also analyze the dependence of the apparent permeability to the thickness. As for the low induction levels, the thickness has got a very small impact onto the magnitude and the apparent permeability (see Figure 18).

4.1.3. Iron losses

In Figure 19, the energy loss density is finally calculated as a function of the thickness ζ; and we check again that the losses are increased for thicker electrical sheets made of GO SiFe due to coarser magnetic structures.

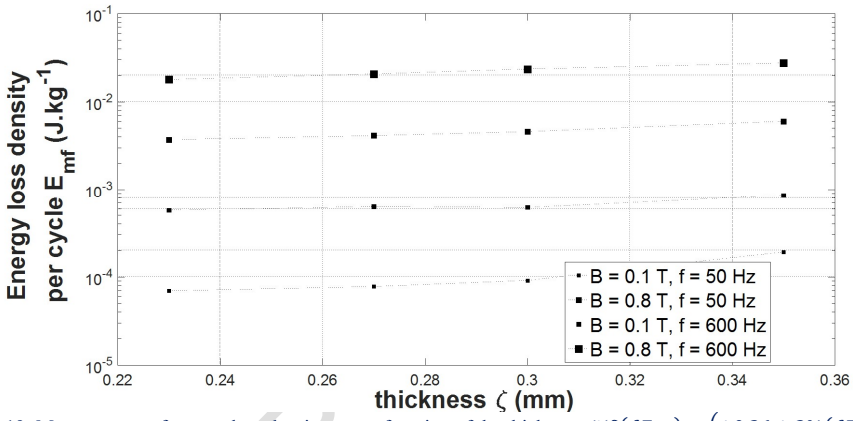

Figure 19: Measurement of energy loss density ■ as a function of the thickness ζ ($\delta(fE_{mf}) = (\pm 0.26 \pm 3\%(fE_{mf}))\,[mW/kg]$).

4.2. Presentation of global results at high induction

4.2.1. Hysteresis loops

Thanks to the accurate identification of $\mu(H_M)$ and $\Lambda(H_M, \partial_t H_M)$, the hysteresis loops can be also reproduced at higher induction levels, i.e. with non-linear assumptions (see Figure 20). Significant discrepancies can be noticed still for negative and high flux densities and close to saturation and the residual induction. It should be possible to improve this by adding the contribution of a static hysteresis model $H_s(H_M, dH_M)$.

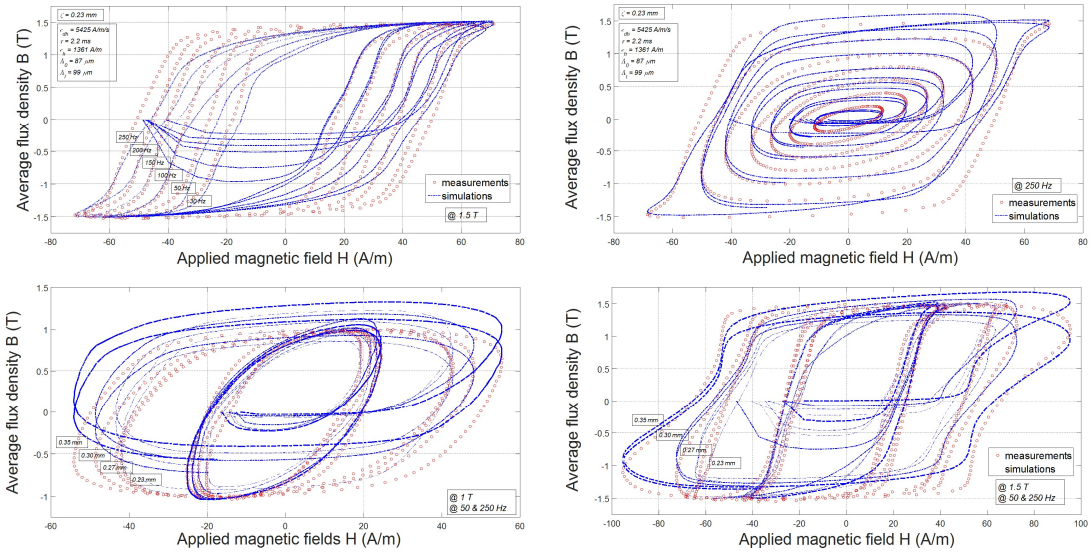

Figure 20: Measurement and computation of hysteresis loops computed at high induction thanks to the non-linear properties. Experimental errors for H and B can be found in the *Appendix 2* ($\delta H = (\pm 1.5 \pm 2\%H)[A/m]$ and $\delta(fB) = (\pm 0.21 \pm 2\%(fB))[T.Hz]$).

One of the partial conclusion of this paper is that providing a knowledge concerning the variations of $\mu(B \text{ or } H_M)$ and $\Lambda(B \text{ or } H_M, \partial_t B \text{ or } \partial_t H_M \text{ or } f, \zeta)$ as a function of the working conditions, mainly the induction level B and its time derivative $\partial_t B$ or the frequency f, but also and more especially as a function of the sheet thickness ζ, it is possible to estimate with sufficient accuracy the total magnetic losses within both magneto-harmonic and transient working conditions from low to high induction levels with saturation and with frequencies from 50 to 800 Hz. Thanks to the accurate identification of $\mu(H_M)$ and $\Lambda(H_M, \partial_t H_M, \zeta)$, the hysteresis loops can be also reproduced with accuracy at low and intermediate induction levels for the same frequencies between 50 Hz and 800 Hz. The computation of hysteresis at higher induction levels are less accurate and requires to add the contribution of a static hysteresis model $H_s(H_M, dH_M)$ especially for the lowest thickness. The study of the thickness ζ dependence of Λ at the macroscopic scale by analyzing the variation of losses shows that the dynamic magnetization property is most of cases reduced when the thickness is lowered. This result suggests a domains refinement effect by reducing the sheet thickness. The goal of the next and last section is to correlate the thickness ζ dependence of Λ with the changes in the magnetic structure and associate properties thanks to the Magneto-Optical Indicator Film (MOIF) technique.

5. Magneto-Optical Indicator Film images of GOES samples

5.1. The samples

In the following, we propose to observe and analyze the magnetic structure of the GO SiFe steel (@TKES*) laminated with the same four different thicknesses as before. The whole specimens were manufactured with the same initial chemical composition (SiFe with 3% of Si), the same recrystallisation process and the same coating process. Epstein samples (with dimensions 30*300 mm^2) with a stress releasing annealing after cutting were still used. Magnetic observations were performed on sample surface with the four thicknesses (ζ = *0.23 / 0.27 / 0.30 / 0.35 mm*). We saw previously that the typical grains' size (15-35 mm) and orientation (6° max disorientation) are more or less the same from one sample with one thickness to another sample with another thickness. The coating process is unchanged and gives rise to two inorganic thin layers, one layer of glass-film and one layer of phosphate based insulator (2-4 µm thick). The aim of this end section is both to check the average grains' size and evaluate the domains width as a function of the sheet thickness.

5.2. The experimental set-up – MOIF (Magneto-Optical Indicator Film) camera

The experimental set-up used is a magneto-optical camera equipped with a polarized light source, a Faraday effect sensor based on the thin Magneto-Optical Indicator Film sensitive to very low field strength, down to 2 mT, and a resolution from 10 to 20 um and a precision of 20 um, and an active-pixel CMOS type image sensor based on MOSFET (MOS Field Effect Transistors) coupled to dichroic analyzers able to separate linear polarizations.

5.3. Observation of the grains size and the surface magnetic structures – analysis of the domains width

The MOIF images clearly show grains' boundaries with discontinuities of domains' shape and directions across them (see Figure 22). By analyzing the smallest and larger grains in Figure 21, it is possible to conclude that there is no significant dependence of the grains 'size on the sheet thickness. With this technique, it is not possible to know with accuracy the grains' orientation, it is however possible to check that the average misorientation of grains stays below 3-6°. This misorientation is inducing the domains' refinement while decreasing the thickness due to magnetic poles at the top and bottom surfaces. Let's then measure the domains' width as a function of the thickness.

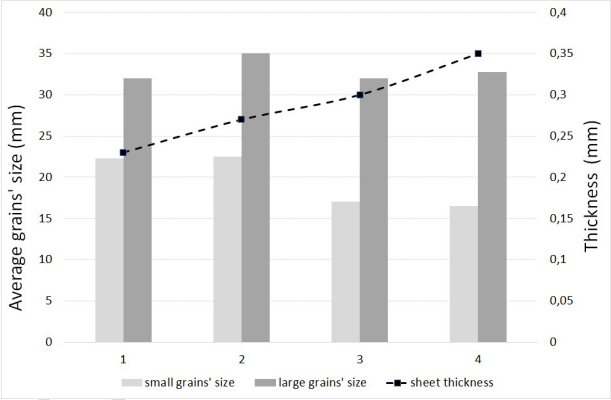

Figure 21: No dependence of the typical grains' size on the sheet thickness.

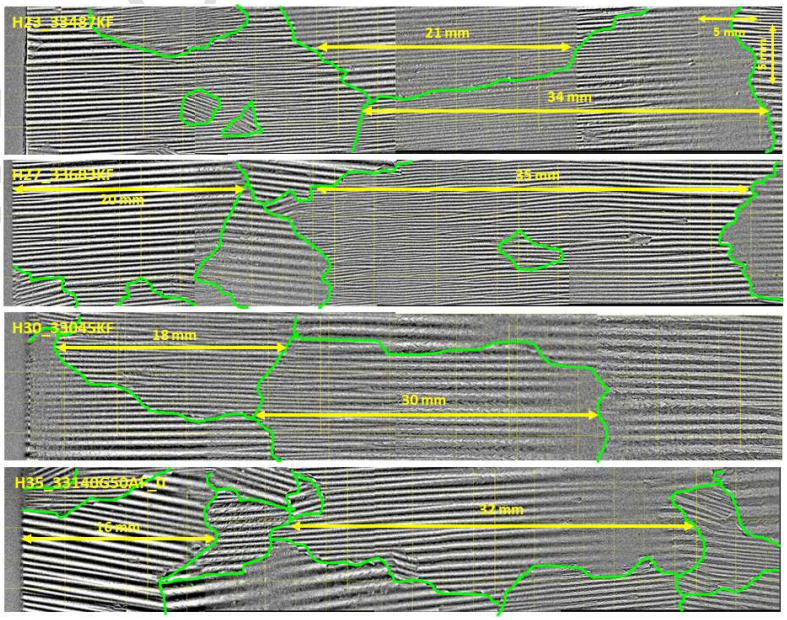

Figure 22: MOIF (Magneto-Optical Indicator Film) images of magnetic domains on samples with four different thicknesses (0.23 / 0.27 / 0.30 / 035 mm). The grains' size and boundaries, limiting the domains, can also be observed on the images (grains' size between 15 and 35 *mm*).

The observation of magnetic domains with the MOIF technique allows to estimate the statistical average of domains' width l_w defined in equation (32). In fact, MOIF images of domains can be analyzed with the FFT technique in 2D (see Figure 23). The geometrical parameter l_w is thus obtained thanks to the median value $\bar{k}$ of spatial frequency k in the probability density spectra of the domains' size in the transverse direction .

$$l_w = \frac{1}{n_w s_w} = \frac{1}{2\bar{k}} \tag{32}$$

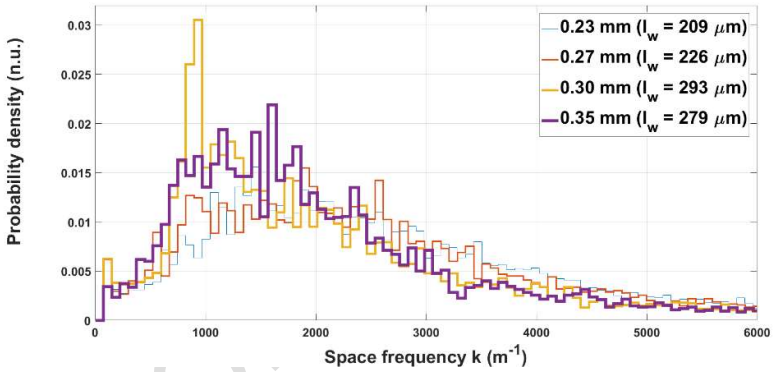

Figure 23: Probability density spectra as a function of the space frequency of magnetic domains in the transverse direction.

5.4. Analysis of domains width and walls' mobility for various thicknesses - discussions

The magnetic analysis described previously, with both experimental data and modeling tools, allows the identification of the dynamic magnetization property Λ, which lumps fundamental microscopic information. At extremely low magnetic field and without time variations, we consider that Λ, closely linked to the magnetic structure characteristics at static equilibrium without macroscopic magnetization, is approximately given by equation (33).

$$\Lambda = \Lambda_0 + \Lambda_l \approx \Lambda_{DWD} \overset{\substack{J_{//} \approx B_{//} \\ J_{\perp} \approx B_{\perp} \approx 0 \\ \eta_{wa} = \eta_w \frac{n_{wa}^2 A_w^2}{n_w^2 s_w^2}}}{\approx} \sqrt{\frac{1}{2\sigma \eta_{wa} n_w s_w J_s}} \tag{33}$$

As a consequence, by measuring the domains' average width l_w thanks to the MOIF technique at one side and by identifying Λ at the other side, it is possible to conclude about the physical origins of iron loss reduction when the sheet is thinner. This loss reduction is not only due to the weakening of eddy current loss within the skin effect, but it can also be due to the domains' refinement induced by surface magnetic poles probably due to the small misorientation of grains. Meanwhile, the active walls' mobility given by (34) can either be enhanced depending on the distancing of walls (size of domains) or weakened due to the spreading surface of walls in the thickness.

$$\eta_{wa} = \eta_w \frac{n_{wa}^2 A_w^2}{n_w^2 s_w^2} = \frac{l_w}{2\sigma J_s \Lambda^2} \tag{34}$$

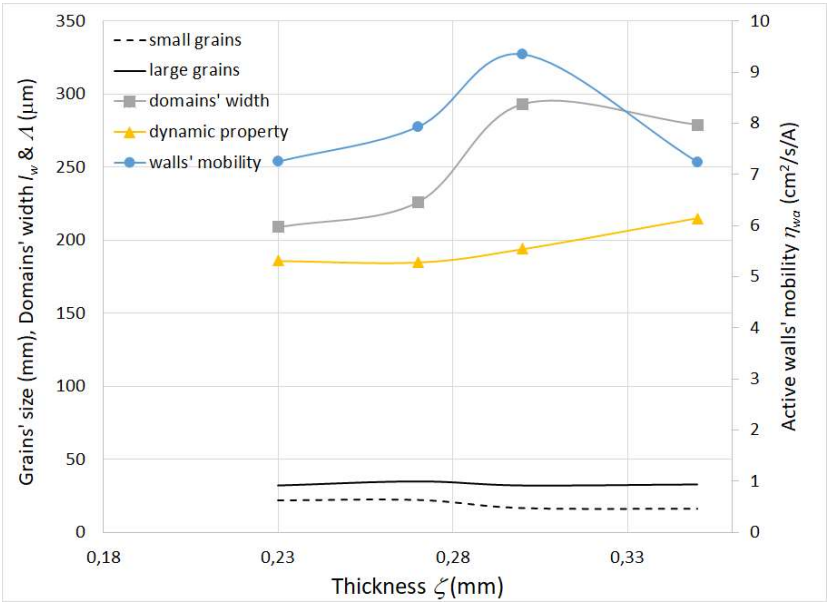

Figure 24: separated identification of property Λ, the domains' width l_w and the walls mobility η_{wa}.

6. Discussion and conclusion

As a conclusion, the dynamic field diffusion like equation for electrical steels seems to suit both NO SiFe steels [17, 25, 26] and GO SiFe materials (present paper). This model is based on the microscopic eddy currents and the corresponding anti eddy field that appear around domains walls and inside the domains during the domain walls displacement and the domains magnetization rotation. Therefore, a connection can be clearly established between the measurable observables and the microscopic magnetization reversal properties. For this purpose, a mesoscopic dynamic magnetization property called Λ is defined and identified for both low induction and high induction levels. Any non-linear variations of the microscopic properties related to any magnetization reversal mechanisms (walls bowing, multiplication, nucleation, fusion …) can be represented in the property Λ as a function of the magnetic state (*i.e.* the flux density B or the static anhysteretic field H_M) and its first time derivative ($\partial_t B$ or $\partial_t H_M$). The experimental identification of the linear property at low induction can be done by fitting the magnetic losses. The results reveal that Λ is a decreasing function of B and f due to the non-linear reversal mechanisms. At the same time, the values for NO materials are usually higher than for GO materials. This is probably due to the low walls' mobility and surface in NO materials. The experimental identification of the non-linear property at high induction can be done by fitting the whole hysteresis loops. The result is usually a cloud of numerous data that must be modeled with a statistic distribution of walls population as a function of H_M and its first time derivative $\partial_t H_M$. The choice of the statistic distribution depends on the material and it is already not the same for NO [17, 25, 26] and GO materials [32]. However, in any case, Λ is still a decreasing function of the dynamic field, a combination of H_M and its first time derivative. Above all, the goal of this paper was to examine the geometry dependence of static and dynamic magnetization properties. The dynamic contribution of the complete behavioral model has been carefully examined, and the results obtained for the hysteresis loops at high inductions show that it is necessary to add the static hysteresis contribution and to improve the non-linearities of both μ and Λ in order to increase the accuracy of predictions. No conclusion can be given proposed for low frequencies below 30 Hz, and the main conclusions concern frequencies between 50 and 800 Hz, frequencies for which giving more importance to the dynamic losses in front of static losses usually makes sense. In this model, there is no separation of classical losses and excess losses, the whole frequency dependent losses are due to eddy currents induced by dynamic magnetization reversal processes and the field diffusion like process involved in a single contribution. After having identified the properties μ and Λ, it is however possible to identify separately the microscopic average walls mobility thanks to the observation of magnetic domains width. Iron losses are not exclusively dependent on the sheet thickness but also on the magnetic domains width and walls mobility. This paper shows that the internal static permeability μ does not significantly depend on the sheet thickness. However, the dynamic magnetization Λ is highly sensitive to the sheet thickness due to surface conditions. The reasons for this sensitivity have been discussed in case of a GO steel with a coating, a tensile stress and possible closure Lancet domains or/and surface magnetic poles. This thickness dependence is probably due to a domain refinement effect induced by surface magnetic poles apparently due to the small misorientation of grains. The field diffusion process is governed by the sheet thickness whereas the dynamic magnetization is determined by the domains width and walls mobility. Both have got a significant impact on the magnetic losses. Thank to the present work, we can identify the metallurgical and magnetic reasons for the thickness dependence of the magnetic structure. This sensitivity is closely related to a coupling between grains size, orientation (texture) and surface effects. A relative control of these surface effects is investigated elsewhere through surface laser treatments. Finally, any geometry dependence and spatial heterogeneity in Λ itself requires more development on a new model for the magnetic structure and its reversal mechanisms [27, 28, 33].

Bibliography

[1] F. Bitter, *Phys. Rev.*, Vol. 38 (1931), pp. 1903.
[2] P. Weiss, ''L'hypothèse du champ moléculaire et la propriété ferromagnétique'', *Journal de Physique*, vol. 6, p. 661, 1907.
[3] P. Weiss, *J. Phys. Theor. Appl.*, 6 (1) (1907), pp.661-690.
[4] R.H. Pry, C.P. Bean, *J. Appl. Phys.*, vol. 29 (1958), 532-533.
[5] Ch. P. Steinmetz, "On the law of hysteresis", reprint, Proc IEEE, 72(2), pp. 196 -221, 1984.
[6] J. Reinert, A. Brockmeyer, R.W.De Donker,"Calculation of losses in Ferro- and Ferrimagnetic materials based on the modified Steinmetz equation", IEEE Transactions on Magnetics, vol. 37(4):p.1055-1060, 2001.
[7] G. Bertotti, "General Properties of Power Losses in Soft Ferromagnetic Materials", *IEEE Transactions on Magnetics*, 1980, vol. 24(1), pp. 621-630.
[8] V. Basso, G. Berttoti, O. Bottauscio, F. Fiorillo, M. Pasquale, ''Power losses in magnetic laminations with hysteresis: Finite element modeling and experimental validation'' J. Appl. Phys. 81 (8), 15 April 1997.
[9] Afef Kedous-Lebouc, Thierry Chevalier, "Loss Surface (LS) Model for iron loss prediction in electrical machines", *International conference on Materials for Electrotechnique and IEEE Romanian Magnetic Society Chapter MmdE & IEEE ROMSC*, Jun 2006, Bucarest, Romania.
[10] F. Preisach, "Über die magnetische Nachwirkung", *Zeitschrift für Physik*, 1935, Bd. 94.
[11] I.D. Mayergoyz, G. Friedman, "Generalized Preisach Model of Hysteresis", *IEEE transactions on Magnetics*, 1988, vol. 24(1): p. 212-217
[12] D.C Jiles and D.L Atherton, "Theory of ferromagnetic hysteresis", Journal of Magnetism and Magnetic Materials, Vol. 61, pp. 48-60, 1986.
[13] D. C. Jiles ''Modelling the Effects of Eddy Current Losses on Frequency Dependent Hysteresis in Electrically Conducting Media'' IEEE Transactions On Magnetics, Vol.30. No.6, Novembre 1994
[14] T. Chevalier, A. Kedous-Lebouc, B. Cornut, C.Cester ''A new dynamic hysteresis model for electrical steel sheet'' Elsevier Science, Physica B 275 (2000) p:197-201
[15] M-A. Raulet, B. Ducharne, J-P. Masson, and G. Bayada, "The magnetic field diffusion equation including dynamic hysteresis", *IEEE Transactions on Magnetics*, 2004, vol. 42, n°2, pp. 872–875.
[16] O. Maloberti et al., "An energy-based formulation for dynamic hysteresis and extra-losses", *IEEE Transactions on Magnetics*, vol. 42, n°4 (2006), pp. 895-898.
[17] O. Maloberti et al., "Hysteresis of Soft Materials Inside Formulations: Delayed Diffusion Equations, Fields Coupling, and Nonlinear Properties", *IEEE Transactions on Magnetics*, vol. 44, no6 (2008), pp. 914-917.
[18] L. Landau, E. Lifshits, "On the theory of the dispersion of magnetic permeability in ferromagnetic bodies", Reprinted from *Phys. Zeitsch*. der Sow. 8 (1935), pp. 153–169.
[19] L. Weil, *Le journal de physique et le radium*, Tome 12 (1931), pp. 437-447
[20] B. Thomas, "The influence of material thickness on the magnetic properties of Co-Fe-V alloy", IEEE Transactions on Magnetics, vol. 17, no. 5, pp. 2470 - 2479, 1981.
[21] Y. Yamashiro, Y. Yoshida, N. Teshima, K. Narita, "Thickness dependence of magnetic properties in rapidly quenched 6.5 percent silicon iron thin ribbons", IEEE Transactions on Magnetics, vol. 18, no. 6, pp. 1421 – 1423, 1982.
[22] Y. Yoshizawa, K. Yamauchi, "Induced Magnetic Anisotropy and Thickness Dependence of Magnetic Properties in Nanocrystalline Alloy "Finemet", IEEE Transactions on Magnetics, vol. 5, no. 11, pp 1070 – 1076, 1990.
[23] M. A. Raulet & al, "Test of the sample geometry independence of a dynamic hysteresis behavioural model of magnetic materials", *Journal of Magnetism and Magnetic Materials*, 2000, vol. 215-216, pp. 620-622.
[24] J. Schneider, S. Reichelt, A. Stöcker, B. Fachmann, and R. Kawalla, "Frequency Dependence of Magnetization Behavior for FeSi Materials with Different Thickness", IEEE Transaction on Magnetics, Vol. 48, NO. 4, pp 1429-1432, Avril 2012.
[25] Olivier Maloberti ''Contribution a la modélisation de la dynamique d'aimantation dans les matériaux magnétiques doux : caractérisation et simulation'' Electric power. Institut National Polytechnique de Grenoble-INPG; France, 2006.
[26] O. Maloberti, A. Kedous-Lebouc, O. Geoffroy, G. Meunier, and V. Mazauric, "Field Diffusion-Like Representation and Experimental Identification of a Dynamic Magnetization Property", *Journal of Magnetism and Magnetic Materials*, 2006, vol. 304, pp. e507-e509.
[27] O. Maloberti, G. Meunier, A. Kedous-Lebouc, V. Mazauric, "How to Formulate Soft Materials Heterogeneity? 1. Quasi-Static Equilibrium and Structuring", submitted to J.M.M.M., conference SMM'18 in Cardiff 2007.
[28] O. Maloberti, A. Kedous-Lebouc, G. Meunier, V. Mazauric, "How to Formulate Soft Materials Heterogeneity? 2. Hysteresis, Dynamic Motions and Diffusion", submitted to J.M.M.M., conference SMM'18 in Cardiff 2007.
[29] J.W. Shilling, JR. L. Houze, "Magnetic properties and domain structure in grain-oriented 3% Si-Fe", Trans. on Magnetics, vol. MAG-10, no. 2, pp. 195, 1974.
[30] Masaaki Inamura, "AC magnetostriction in Si-Fe single cristal close to (110)[001]", IEEE Transactions on Magnetics", vol. MAG-19, no. 1, january 1983.
[31] D.X. Chen, J.L. Muñoz, "Theoretical eddy current permeability spectra of slabs with bar domains", IEEE Transactions on Magnetics, 1997, vol. 33(3): p. 2229-2244.
[32] E. Salloum, O. Maloberti, M. Nesser, S. Panier, J. Dupuy, " Identification and analysis of static and dynamic magnetization behavior sensitive to surface laser treatments within the electromagnetic field diffusion inside GO SiFe electrical steels", Journal of Magnetism and Magnetic Materials, 2019.
[33] O. Maloberti, M. Nesser, E. Salloum, S. Panier, J. Fortin, P. Dassonvalle, C. Pineau, T. Nguyen, J-P. Birat, I. Tolleneer, "The tensor magnetic phase theory for mesoscopic volume structures of soft magnetic materials – quasi-static and dynamic vector polarization, apparent permeability and losses – experimental identifications of GO steel at low induction levels", Journal of Magnetism and Magnetic Materials, 2020.
[34] M. L. Ababsa, O. Maloberti, O. Ninet, "Sensitivity analysis of iron loss and hysteresis models' parameters to the sheets thickness and magnetic polarization according to the quality of GO SiFe", 2DM workshop 15th, Grenoble, France, 2018.

Acknowledgments

Samples with a stress releasing treatment were kindly given by TKES (ThyssenKrupp Electrical Steels). Measurements were carried out by the LSEE and the ESIEE - UNILASALLE Amiens. Modeling and identification tasks were performed at the ESIEE - UNILASALLE Amiens and have received funding from the European Research Council under the European Union's H2020-IND-CE-2016-17/H2020-FOF-2017 Program (Grant Agreement No. 766437).

APPENDIX 1: Boundaries study

The reason for this appendix is the fact that the walls are supposed to disappear when the material is saturated. Thus, the aim of this appendix is to check the consistency of the present model by studying the behaviour of the property Λ when we saturate the material, either in the rolling direction or in the transverse direction. We notice that close to saturation, the domains and walls density tends towards zero, whereas the walls density and surface tends towards the infinity. The fewer the walls are, the higher its mobility is. Consequently, when we saturate the material in both cases, even if the domains and the walls disappear, the property Λ tends towards a finite number that would be zero if the classical limit is relevant.

- Mechanisms & Limits

		GO grain 0°	GO grain θ°	GO grain 0°
GO grain orientation		GO grain 0°	GO grain θ°	GO grain 0°
Magnetic polarization direction		RD	RD	TD
Polarization components		$J_{//} \to J_s$ $J_\perp \to 0$	$J_{//} \to J_s \cos\theta$ $J_\perp \to J_s \sin\theta$	$J_\perp \to J_s$ $J_{//} \to 0$
Walls density	$n_{wa} < n_w$	$\to 0$		
Walls surface	$A_w < S_w$	$\to \infty$		
Walls mobility	η_w	$\to \infty$		
Domains autocorrelation surface	S_{DMR}	$\to 0$	$\to \propto \zeta g$	$\to 0$
• **D**omain **W**alls **D**isplacement $\Lambda_{DWD} = \sqrt{\frac{n_w S_w J_s}{2\eta_w n_{wa}^2 A_w^2 (J_s^2 - J_s^2)}} \left(\frac{\partial_t J_{//} - \frac{J_{//} . \partial_t \left(\sqrt{J_s^2 - J_s^2} \right)}{\sqrt{J_s^2 - J_s^2}}}{\partial_t B_{//}} \right)$		$\to \frac{0}{0} = finite$ $\to 0$ Classical limit	$\to \frac{0}{0} = finite$ $\to 0$ Classical limit	$\to 0$
• **D**omains **M**agnetic **R**otation $\Lambda_{DMR} = \sqrt{S_{DMR} \frac{J_s^2}{J_s^2 - J_{s\perp}^2}} \left(\frac{\partial_t J_\perp}{\partial_t B_\perp} \right)$		$\to 0$	$\to \propto \zeta g \tan\theta$ $\to 0$ Classical limit	$\to \frac{0}{0} = finite$

$$\eta_w = \frac{8\pi^2 S_w J_{s\perp}}{\sigma J_s^2} \left(\iiint \left(\iint_w \frac{(z - z_w)}{|r - r_w|^3} d^2 \right)^2 d^3 r \right)^{-1} \quad ; \quad S_{DMR} = \frac{n_d}{4\pi} \iiint_d \iiint_d G(r', r) d^3 r' d^3 r \text{ , } G \text{ is the Green function}$$

$J_s \approx 2$ T (saturation polarisation), n_w: walls volume density, η_w: wall mobility, S_w: wall area
n_{wa}: active walls volume density, η_{wa}: active wall mobility, A_w: wall effective area, g: grain size, θ: grain orientation (-7°<θ<+7°)

Figure 25: Boundaries study for dynamic properties.

APPENDIX 2: experimental errors analysis

Estimation of the maximum inaccuracies mainly depend on the current I and voltage V measured:

$\delta I = (\pm 2 \pm 1\% I)[mA]$; $\delta V = (\pm 6.5 \pm 1\% V)[mV]$

and on the Epstein frame dimensions defined with 1.7% relative accuracy (N_1=N_2=*700 turns*):

The magnetic path $L = (0.94 \pm 1.7\% L)[m]$ and the cross section $S \geq (6.9 \pm 1.7\% S)[mm^2]$

Then the fields are calculated by: $H = \frac{N_1 I}{L}$ for the magnetic field and $(fB) = \frac{V}{2\pi N_2 S}$ for the flux density variations.

Fields inaccuracies become then $\xrightarrow{propagation} \delta H = (\pm 1.5 \pm 2\% H)[A/m]$; $\delta(fB) = \left(\pm 0.21 \pm 2\% (fB)\right)[T.Hz]$.

The power loss density can be calculated by: $fE_{mf} = \frac{IV}{2\pi\gamma LS}$, which leads to $\xrightarrow{propagatio} \delta(fE_{mf}) = \left(\pm 0.26 \pm 3\% (fE_{mf})\right)[mW/kg]$.

The apparent permeability is given by: $f\,\mu_{app}/\mu_0 = \left(\frac{L}{2\pi N_1 N_2 \mu_0 S}\right)\frac{V}{I}$, which leads to $\delta(f\,\mu_{app}/\mu_0) = \left(\pm 3240 \pm 3\% (f\,\mu_{app}/\mu_0)\right)[Hz]$

The correspondent inaccuracies on the identified properties μ and Λ can be deduced thanks to equations (28) and (26) as follows:

$\delta(fB\Lambda) = \left(\pm 6 \pm 2\% (fB\Lambda)\right)[T.Hz.\mu m]$

$\delta(f\,\mu/\mu_0) = \left(\pm 3240 \pm 3\% (f\,\mu/\mu_0)\right)[Hz]$